DESIGN, FABRICATION, AND TESTING OF A SHEATHED EMBOLIZATION DEVICE

A Thesis

by

ADAM M. ORENDAIN

Submitted to the Office of Graduate and Professional Studies of
Texas A&M University
in partial fulfillment of the requirements for the degree of

MASTER OF SCIENCE

Chair of Committee,	Duncan J. Maitland
Committee Members,	Balakrishna Haridas
	Wayne Hung
Head of Department,	Michael McShane

December 2017

Major Subject: Biomedical Engineering

ABSTRACT

Endovascular embolization is an interventional procedure to seal off diseased vasculature from systemic circulation. Shape memory polymer (SMP) foams are a promising embolic material that can undergo shape change when exposed to stimuli, exhibit a positive healing response, and aid in rapid occlusion. SMP foams are porous materials that are composed of struts and membranes that pose a risk of generating particles during device fabrication or delivery. Herein, a sheathed embolization device (SED) was designed, fabricated, and tested to occlude a left atrial appendage (LAA) and to mitigate the generation of foam particles.

The SED consists of a thin polyurethane membrane that fully encapsulates the SMP foam, and is able to undergo shape change from a compressed state to an expanded state. Material properties of the device were characterized with differential scanning calorimetry, scanning electron microscopy, and Fourier transform infrared spectroscopy. The SED was tested in terms of its ability to occlude a patient-derived LAA model, its deliverability, and its ability to reduce particles.

Results from the studies demonstrate the SED's ability to be delivered minimally invasively, reduce particles, and occlude mock vasculature. Upon actuation in body-temperature fluid the SED achieved a 10x diameter expansion, making it ideal for endovascular applications. These preliminary results support the potential to utilize SEDs to occlude vasculature while mitigating the risk of unintended ischemia due to device-based particles. The results also demonstrate the potential to integrate the SED with third-

party devices or components to develop functional embolization devices, such as left atrial appendage closure devices.

ACKNOWLEDGEMENTS

I left my home to begin my studies at Texas A&M quietly before the sun could peek above the mountains. The previous night my dad helped me strap down my belongings in the back of my truck. My mom was shining a flashlight while we worked. It was dark and last minute. When we were finished my parents said goodnight, and hugged me knowing I would be gone before they awoke.

Thank you mom and dad for being supportive. I know I do not always follow the recommended path, but regardless, you still extend your love.

I would also like to acknowledge my close friends who have listened to me complain, joined me in misguided adventures, and kept me properly imbibed …with friendship. David, you were my personal therapist and sanity checker whilst we tried to make gains at the rec center. Mauri, you were a great host for our GoT watch parties and Halloween. Joey and Katie, thank you for hosting our cheese, cracker, and salami parties. To my friends in AGEP, BTD, and ASTEP; thank you for taking me out of my bubble in the Biomedical Engineering department. Lastly, thank you to my friends back in Arizona. Richie and Chang, you two both made the trek to Texas. Richie, sorry for getting the flu as soon as you arrived. I still enjoyed your time here, and am so grateful your lovely wife made me chicken noodle soup. Peter and Vanessa, you both were so hospitable whenever I flew into Phoenix. I know navigating the Sky Harbor terminals and Phoenix freeways is not ideal, yet you both chauffeured me around, fed me, and offered me a bed to rest on. I

am indebted to your generosity. Leo; there is no one on Earth like you. We always thought you were ahead of your time back in high school. Thanks for the memes.

Rachelle, I wish I met you sooner. You and your family have been an unexpected yet unsurmountable pillar of support. You are so kind, caring, intelligent, confident, punny, and funny; the true trademarks of a great physician. We have had so many adventures, ups and downs, and all in such a small amount of time. There is no one else I would want to share those moments with.

Lastly, I would like to acknowledge my committee members and colleagues in the Biomedical Device Lab. The caliber of students in the Biomedical Device Lab was beyond compare. Just being surrounded by you all was great insight into the inner workings of highly motivated, ambitious, and successful people. In particular, Dr. Keller spent many hours reviewing my work, and was always approachable. Thank you Dr. Maitland for providing a well-equipped lab and guidance for the development of medical devices. It has been an interesting journey, but I have learned a lot about myself and engineering.

CONTRIBUTORS AND FUNDING SOURCES

This work was supported by the creative insight of Dr. Duncan Maitland, who provided ample guidance to take this thesis from a simple concept to a tangible device, and my committee members, Dr. Balakrishna Haridas of the Department of Biomedical Engineering and Dr. Wayne Hung of the Department of Engineering Technology and Industrial Distribution.

Characterization of various polymers and assistance with tests and equipment was provided by members of the Biomedical Device Lab; in particular Dr. Mary Beth Browning Monroe for performing and analyzing ATR-FTIR spectroscopy, Dr. Mark Wierzbicki and Dr. Brandis Keller for overall instruction, and Justin Feldt for analysis and testing.

Graduate study was supported by the NSF LSAMP Bridge To The Doctorate (BTD) fellowship under grant number HRD-1406755, a Diversity Fellowship from Texas A&M University, and an Enrichment Fellowship from the Department of Biomedical Engineering. The contents of the following thesis are solely the responsibility of the authors and do not necessarily represent the official views of the aforementioned funding sources.

NOMENCLATURE

ATR-FTIR	Attenuated total reflection – Fourier transform infrared
ACP	Amplatzer cardiac plug
CT	Computed tomography
DI	Deionized
DPI	Dots per inch
DSC	Differential scanning calorimetry
HDI	Hexamethylene diisocyanate
HPED	N,N,N’,N’-tetrakis(2-hydroxypropyl) ethylenediamine
GUI	Graphical user interface
ID	Inner diameter
IPA	Isopropyl alcohol
L	Large
LAA	Left atrial appendage
LAAC	Left atrial appendage closure
M	Medium
OD	Outer diameter
PBS	Phosphate buffer solution
PET	Polyethylene terephthalate
PTFE	Polytetrafluoroethylene
S	Small

SS	Stainless steel
SED	Sheathed embolization device
SEM	Scanning electron microscopy
SMP	Shape memory polymers
TEA	Triethanolamine
T_g	Glass transition temperature
T_m	Melt transition temperature
TPU	Thermoplastic polyurethane
USP	United States Pharmacopeia

TABLE OF CONTENTS

LIST OF FIGURES

LIST OF TABLES

1. INTRODUCTION

1.1 Shape memory polymer (SMP) foams

Polyurethane SMP foams are attractive materials for endovascular applications. SMP foams are capable of being compressed to fit inside a catheter and then actuating once exposed to body heat and water inside vasculature, achieving up to a 70-fold volume expansion [1]. SMPs consist of net points and switching segments that are responsible for shape change. To program SMPs, the material is heated above its glass transition (T_g) temperature, and an external stress is applied to deform the material to its secondary shape. The secondary shape is then fixed by cooling the material under constant load. When exposed to a stimuli, the material returns to its primary shape (**Figure 1.1**) [2].

The porous architecture of the foams provides a large surface area for rapid clotting and connective tissue infiltration [3]. Polyurethane based SMP foams have also been shown to be biocompatible in a porcine animal model, producing a reduced inflammatory response when compared to suture materials (silk and polypropylene), cellular infiltration, and endothelialization [4]. These materials are also highly tunable to cater to specific endovascular applications, and have been shown to achieve complete occlusion within 5 minutes [3].

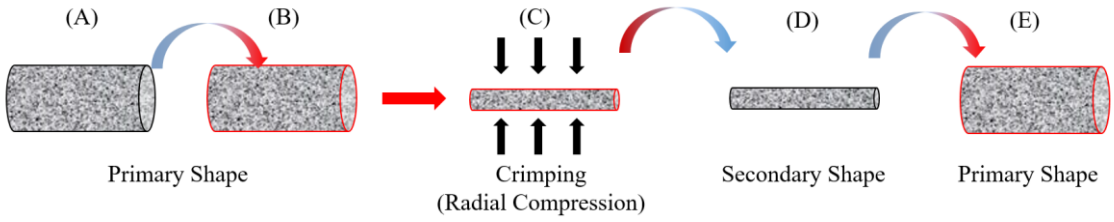

Figure 1.1: Programming SMP materials. (A) The primary shape is (B) heated above its T_g. (C) An external stress is applied and held while (D) the material is cooled below its T_g. (E) Heating the SMP material above its T_g causes the material to actuate and return to its primary shape.

1.2 Left atrial appendage closure

Closure of the left atrial appendage is a treatment option for patients suffering from atrial fibrillation to reduce their risk of stroke. Atrial fibrillation (AF) is an abnormal heart rhythm that is associated with significant morbidity and mortality. It affects roughly 6.1 million in the USA, which is expected to increase to 12 million by 2050 [5]. Patients suffering from AF have an irregular heart rhythm that results in a pooling of blood in the atria and formation of clots in the appendage (**Figure 1.2)**. The formation of clots increases risk of stroke, which is the third leading cause of death in the USA [6]. Data suggests that 15% of all strokes are attributable to AF [7]. In the mid-1950s, it was found that the majority of clots in patients with AF were formed in the LAA. This discovery stimulated the development of LAA exclusion treatments [5].

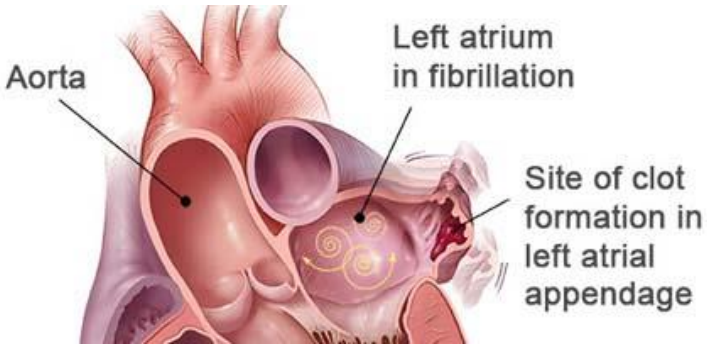

Figure 1.2: Clot formation in the left atrial appendage as a result of atrial fibrillation [8].

Presently, the treatment of choice for preventing stroke in AF patients is oral anticoagulation therapy. However, oral anticoagulation therapy is not well tolerated by patients due to its interaction with other medications, potential for bleeding, and narrow therapeutic window [9-11]. Given that fewer than 50% of patients with AF are considered candidates for oral anticoagulation therapy, and that the LAA is the source of 90% of atrial thrombi, LAA closure is a desirable treatment [12]. LAA closure can be performed surgically or percutaneously with epi- or endo-cardial devices (**Figure 1.3**) [13].

Percutaneous closure of the LAA is associated with a less invasive procedure, a faster recovery time, and reduced risk of bleeding. Currently, the WATCHMAN (Boston Scientific) is the only FDA-approved LAA closure device, but several other devices have received CE marking or are in development [13]. In general, these devices are composed of a self-expanding nitinol frame with barbs, or anchors, that exclude the LAA while engaging the surrounding tissue to prevent migration. Complications from these devices include air embolism, pericardial effusions, tamponade, tissue tearing, device embolization, and stroke [11].

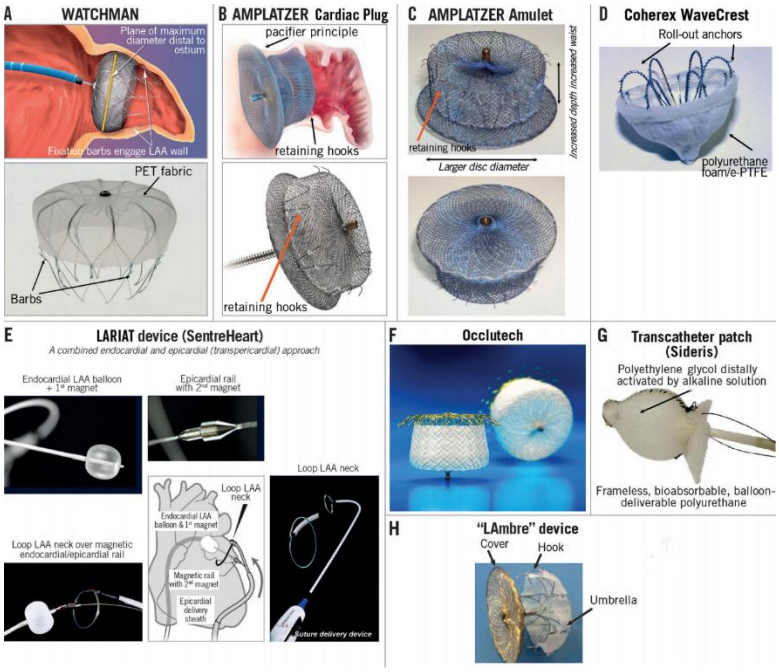

Figure 1.3: Catheter-based LAA occlusion devices used clinically. (A) WATCHMAN (Boston Scientific); (B) AMPLATER Cardiac Plug (St. Jude); (C) AMPLAZER Amulet (St. Jude); (D) Coherex WaveCrest (Coherex Medical); (E) LARIAT (SentreHeart); (F) Occlutech LAA occluder (Occlutech); (G) Transcatheter patch (Sideris); (H) LAmbre (Lifetech Scientific) [13]. Reprinted from Eurointervention, with permission from Europa Publishing.

Partial to full volumetric occlusion of the LAA cavity, as opposed to just sealing the entrance to the appendage, may improve outcomes. Non FDA-approved devices have partially filled the appendage cavity with polyester mesh, nitinol mesh, expanded polytetrafluoroethylene (ePTFE), and polyurethane foam [14]. A goal of this thesis is to design an embolization device composed of SMP foam that is capable of occluding a LAA. The proposed embolization device should also be able to integrate with hard materials, like nitinol, to improve fluoroscopic guidance and cavity sealing. A method to protect the SMP foam from hard materials will also be discussed and investigated in this thesis.

1.3 Particulate matter

Particulates are “mobile undissolved particles [that are] unintentionally present” in media [15]. The FDA requires medical device manufacturers to evaluate the size and amount of particulates generated by device materials, manufacturing processes, and the final device [16, 17]. Implanted devices that are upstream of brain vasculature pose an unique and significant risk of generating particulates that can cause transient ischemic attacks or strokes [18]. Therefore, procedural or device controls are needed to mitigate the risk.

The intended application and design of the embolization device discussed in this thesis is especially at risk for generating harmful particulates. To mitigate the risk and generation of device-related particulates, a thin polymeric membrane will encapsulate the SMP foam and serve as a barrier and emboli protector. An adapted protocol will then quantify the amount of generated particulates and verify the membrane is functional.

1.4 Approach

Incorporation of SMP foam in a LAA closure device may result in rapid clotting, endothelialization, and tissue ingrowth that biologically fixates the device within the appendage. As a result, adverse events, such as device thrombosis, device migration, and incomplete occlusion may be reduced. Current devices generally lack a volume filling occlusion member, and serve their function of preventing stroke by sealing the ostium of the LAA.

To improve volume occlusion, a device comprised of SMP foam encapsulated within a membrane will be fabricated. The sheathed SMP occlusion device can then be integrated into existing devices or be used individually to embolize vasculature. The encapsulated SMP foam can be attached to proximal and distal marker bands to enable fluoroscopic guidance and device delivery. The membrane will function as a filter between the SMP foam and surrounding environment to capture any foam particulates that are generated during delivery. The membrane may also aid in endothelialization of the device. Additional features include a detachment mechanism that can connect to a delivery cable. The proposed device is intended to improve occlusion times, reduce particulate generation, and serve as an adjunct for predicate occlusion devices.

1.5 Summary of thesis

An SMP-based embolization device that can be integrated with hard materials, without increasing the generation of device-related emboli, is highly desirable. A potential application of an embolization device comprised of SMP foam and nitinol is the closure of LAAs. With that in mind, the goals of this thesis is to design, fabricate, and test a sheathed embolization device (SED) that is capable of occluding a LAA and mitigating the generation of device-related emboli.

Chapter 2 discusses suitable SMP foams to occlude a LAA. Criteria for foam to be successful in the endovascular embolization of the LAA is discussed and investigated. A method to maximize the expansion ratio of foam is introduced and investigated. The thermal properties of SMP foam is characterized with differential scanning calorimetry

(DSC) and reported. The morphology of SMP foam is visualized with light microscopy and scanning electron microscopy (SEM), and its impact on endovascular outcomes is discussed. Lastly, the rate at which SMP foams actuate at body temperature is investigated as a function of its geometry.

Chapter 3 describes the rationale, design, and fabrication of a SED. The design of the device is based on predicate devices that are used for LAA closure, and is presented. A thorough literature review highlights materials that are used in cardiovascular applications, such as capturing emboli or occluding LAAs. Several materials are investigated for their potential use to encapsulate SMP foam. Several processes, such as thermoforming, are discussed in relation to fabricating devices. A suitable material is selected to function as membrane to encapsulate SMP foam and capture emboli. The chemical, thermal, and morphological properties of the membrane material is characterized and presented. The final device composition and fabrication process is presented and justified.

Chapter 4 describes the test methods and testing of the final device. The crimped diameter of the devices were recorded and evaluated for their ability to be delivered minimally invasively. Crimped devices were submerged in bovine blood to determine if the devices actuate or form thrombus. Adsorption of blood and formation of thrombus was analyzed gravimetrically and visually with SEM. Devices were also delivered into an anatomic model of the LAA. The anatomic model was based on computed tomography (CT) data from a human patient. Gaps between the device and appendage opening was quantified with image processing. Qualitative features of delivery such as difficulty,

device recapturing, and device deployment are reported. Lastly, particle generation from SMP foam and SMP foam encapsulated by a membrane is reported. The particle protocol is adapted from a guidance document from the United States Pharmacopeia (USP).

2. SHAPE MEMORY POLYMER CHARACTERIZATION

2.1 Introduction

Identification of suitable SMP foam is essential to producing a high-performance implantable medical device. Certain characteristics SMP foam should possess for use in endovascular occlusion applications include: the ability to remain stored in their secondary configuration, the ability to volumetrically fill cavities upon exposure to a stimuli, positive blood and tissue interactions, and a tailored actuation profile. In this chapter several characterization techniques were employed to characterize the thermal properties that regulate the shape change of SMP foam, as well as the geometric architecture of SMP foams.

The results from this chapter will aid in the design and development of an embolic device that can potentially be used to occlude LAA's. The purpose of the SMP for this application is to volumetrically fill the LAA cavity in a reasonable manner, then subsequently allow rapid and stable thrombus formation within the cavity. Over the span of 90 days the exposed surfaces of the SMP foam should become endothelialized, forming a neointima at the ostium of the LAA. Rodriguez et al. have demonstrated SMP foams ability to form discontinuous and continuous endothelial layers at 30 and 90 days, respectively, in a porcine aneurysm model. Further, cellular, connective, and granular tissue infiltration is observed within the SMP foam scaffolds, suggesting an active healing response [4]. Herein, several SMP foam geometries will be investigated for their ability to be delivered via traditional procedural techniques and their ability to fill a large LAA.

2.2 Materials and methods

2.2.1 SMP synthesis

Polyurethane SMP foams were synthesized following a three-step protocol previously described by Hasan et al. [19]. Briefly, isocyanate prepolymers composed of appropriate molar ratios of N,N,N',N'-tetrakis(2-hydroxypropyl)ethylenediamine (HPED, 99%; Sigma-Aldrich Inc., St. Louis, MO), triethanolamine (TEA, 98% Sigma-Aldrich Inc.), and hexamethylene diisocynate (HDI, TCI America Inc., Portland, OR) were synthesized. The isocyanate prepolymer is then reacted with a hydroxyl mixture blended with the remaining molar equivalents of HPED and TEA. The hydroxyl mixture also contained catalysts (T-131 and BL-22, Air Products and Chemicals Inc., Allentown, PA) and deionized (DI) water. To create foams the isocyanate prepolymer and hydroxyl mixture were combined with surfactants (DC 198 and DC 5943, Air Products and Chemicals Inc.), and a physical blowing agent Enovate (Honeywell International, Inc., Morristown, NJ) to create SMP foams.

Foam formulations are denoted as HXX, where "XX" corresponds to the ratio of HPED to TEA equivalents. Varying the ratio of HPED to TEA enables tuning of the thermo-mechanical properties of the foam. Based on previous internal investigations and inventory, a foam composition of H40 was investigated. The mechanical properties of H40 foams used in thesis can be found in Appendix A.

2.2.2 Foam processing

Following foam synthesis, the bulk foam was cut into rectangles that were 7 cm long, 6 cm wide, and 2 cm thick using a hot wire cutter. The rectangular blocks of foam were then placed into fixture and penetrated by an array of pins while subjected to low amplitude, high frequency perturbations. This process, coined reticulation, is described by Rodriguez et al., and allows the creation of an open-cell network (**Figure 2.3A**) that allows blood and cellular infiltration throughout the foam matrix [20].

Cylindrical foams 3 cm in diameter were then cut from the reticulated foam rectangles using a 3D printed hole puncher. A 3 cm foam diameter was chosen to treat large LAA cavities, and approximates the size of large LAA closure devices. By approximating large LAA closure devices we can simulate the "worst-case" scenario for delivery and match industry standards. LAA closure devices are typically oversized by 9 to 30% relative to the maximum LAA ostium diameter; therefore a SED with a 3 cm outer diameter (OD) may occlude a LAA with an ostium of approximately 23 to 27.5 mm [13, 14].

The center of the cylindrical foams were then bored out with disposable biopsy punches (Sklar Surgical Instruments, West Chester, PA, USA) or with custom hole punchers, resulting in hollow cylinders (**Figure 2.1**). The centers were bored out to enable delivery through smaller catheters and to maximize expansion ratios. **Table 2.1** outlines the foam geometries investigated in this thesis.

Table 2.1: Investigated H40 foams. Small, medium, and large (S, M, and L) designations correspond to pore sizes of approximately 1000, 1500, and 1800 μm, respectively. Foams of each pore size will have 0 to 20 mm bores in the center.

Pore Size (μm)	~1000 (Small)					~1500 (Medium)					~1800 (Large)				
Bore Size (mm)	0	5	10	15	20	0	5	10	15	20	0	5	10	15	20

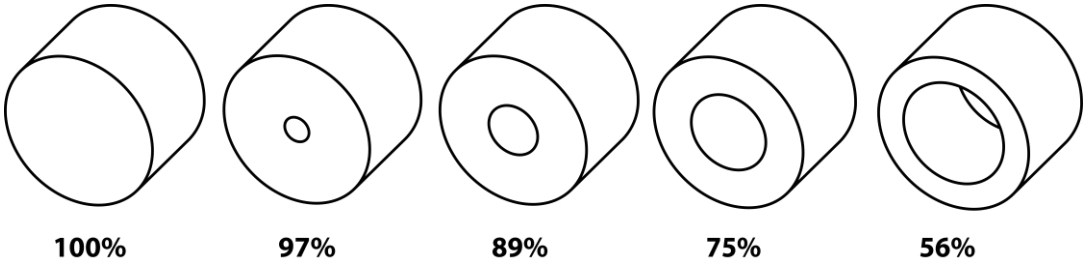

Figure 2.1: H40 SMP foams (30 mm OD x 20 mm length) with increasing bore diameter. From left to right, 0, 5, 10, 15, and 20 mm bore diameters. The percent below the foam indicates the volume relative to the non-bored foam.

After the foams were cut into their final geometry, they were cleaned to remove unreacted monomers, plasticizers, and particulates. A cleaning cycle consisting of submerging foam in 99% isopropyl alcohol (IPA, VWR, Radnor, PA) and rinsing with reverse osmosis (RO) water under sonication was performed and described in **Table 2.2**. The amount of solvent used was approximately 20x the volume of foam. After cleaning, the foams were placed in aluminum trays with RO water and allowed to freeze in a -20°C freezer for 12 h before freeze-drying in a FreeZone Freeze Dryer (Labconco, Kansas City, MO) for 24 hours.

Table 2.2: Description of foam cleaning process.

Cleaning Step Name	Time	Description of Method
RO Sonication	30 min	Foams sonicated with RO water at 37°C in beaker
IPA Sonic 1	30 min	Previous solvent removed. Foams sonicated with IPA at 37°C
RO Rinse 1	1 min	Previous solvent removed. Foams rinsed with RO water to remove residual IPA
IPA Sonic 2	30 min	Foams sonicated with IPA at 37°C
RO Rinse 2	1 min	Previous solvent removed. Foams rinsed with RO water to remove residual IPA
IPA Sonic 3	30 min	Foams sonicated with IPA at 37°C
RO Rinse 3	1 min	Previous solvent removed. Foams rinsed with RO water to remove residual IPA
Final RO Sonic	30 min	Foams sonicated with RO water at 37°C
Final RO Rinse	1 min	Previous solvent removed. Foams rinsed with RO water

2.2.3 Differential scanning calorimetry (DSC)

Each batch of foams synthesized had their dry and wet glass transition (T_g) temperatures characterized using a Q-200 dynamic scanning calorimeter (DSC) (TA Instruments Inc., New Castle, DE). The dry and wet T_g of the foam can help elucidate at what temperatures the foams will actuate at under dry and wet conditions. These temperatures have important implications in terms of storing the foam samples, and understanding the expansion kinetics when the foam is inside the body. In other words, dry and wet T_g can determine whether or not the foam will expand prematurely outside the body; or if it will expand once inside the body.

Foam samples (3-10 mg; N = 3) were taken from already processed foam cylinders. Samples used for dry T_g analysis were hermetically sealed and packed in aluminum pans. The DSC protocol specified an initial sample cooling to -40°C at a rate of 10°C/min, then

holding it isothermally for 2 min. Following the cooling cycle, a heat ramp at a rate 10°C/min to 120°C occurred. The cooling and heating cycle was then repeated twice; the last heating cycle was analyzed to quantify dry T_g values of the foam. The T_g measurement was based on the inflection point of the thermal transition curve using TA Instruments software.

Wet T_g foam samples were submerged in RO water at 50°C for 15 minutes to allow full plasticization. Samples were then removed from water, sandwiched between Kimwipes (Kimberly-Clark Professionals, Roswell, GA), and press dried with a mechanical press (2 tons, 30 seconds). Samples were then weighed (3-10 mg) and placed in aluminum pans with a vented lid. The DSC protocol decreased the temperature to -40°C at 10°C/min and held it isothermally for 2 minutes. The temperature was then increased to 80°C at 10°C/min. The wet T_g measurement was based on the inflection point of the thermal transition curve using TA Instruments software.

2.2.4 Imaging

Foam pore sizes, strut thickness, and cell structure were analyzed by taking magnified images of thin slices of foam using a high resolution light microscope (VHX-5000, Keyence Corporation, Osaka, Japan) and a scanning electron microscope (SEM, Joel NeoScope JCM-5000, Nikon Instruments Inc., Melville, NY). Transverse and axial slices of foam were prepared by cutting foam with a razor-sharp scalpel. Foam samples were mounted onto the light microscope stage and imaged at different magnifications (20x to 200x). Keyence software allowed for real-time depth composition and 2D/3D stitching

of the foam samples, thus providing focused images. Additionally, length measurements of the foam were taken with Keyence software, wherein the pore diameter was taken as the maximum diameter. Ten measurements were taken to account for variation in pore sizes.

SEM samples were prepared by first thinly slicing sections from bulk foam with a razor sharp scalpel. The thin slices were then mounted onto a SEM platform with carbon-tape and placed under vacuum at room temperature overnight. The samples were then sputter coated with gold for 60 s at 20 mA using a Cressington sputter coater (Ted Pella Inc., Redding, CA). Samples were then placed in the SEM chamber and imaged under high vacuum at a voltage of 10 kV or 15 kV.

2.2.5 SMP foam actuation

Actuation, or expansion, studies are performed to characterize how quickly SMP foams will expand inside the body, and how large they will expand. Ideally, the SMP foams should expand in an appropriate time that prevents premature expansion inside the delivery catheter and allows full expansion inside the body cavity.

Prior to performing the actuation studies, crimped foam samples were prepared. Processed SMP foam cylinders described in **Table 2.1** were crimped over a 0.008" nitinol wire using a SC250 Stent Crimper (Machine Solutions Inc., Flagstaff, AZ, USA). The SC250 Stent Crimper was set to a crimping pressure of 80 pounds per square inch (PSI) at 100°C. Foam samples were allowed to equilibrate to 100°C and reach a rubbery state before crimping. Once equilibrated the SC250 Stent Crimper was closed and cooled to

room temperature. The foam samples were then removed and their crimped diameters measured with calipers.

Actuation studies were conducted by loading crimped samples to a fixture, submerging in a heated water bath, and imaging at specific time points. The samples were loaded to a fixture to keep the threaded nitinol wire, and sample, taut. The water bath was heated to approximately body temperature (37.5°C). Samples were then placed into the water bath and imaged every 30 seconds using a digital camera (PowerShot SX230 HS, Canon Inc., Tokyo, Japan) until they foams were fully expanded. The images were then analyzed with either ImageJ (NIH, Bethesda, MD) or an interactive MATLAB program (MathWorks Inc., Natick, MA, USA); the details of which can be found in Appendix B and C.

2.3 Results

2.3.1 Imaging

Light microscopy and SEM imaging revealed foam architecture and the impact reticulation has on foam processing. **Figure 2.2** depicts an open-cell foam that has pore measurements overlaid. SEM images show partially closed-cell and open-cell morphology observed in foam (**Figure 2.3**).

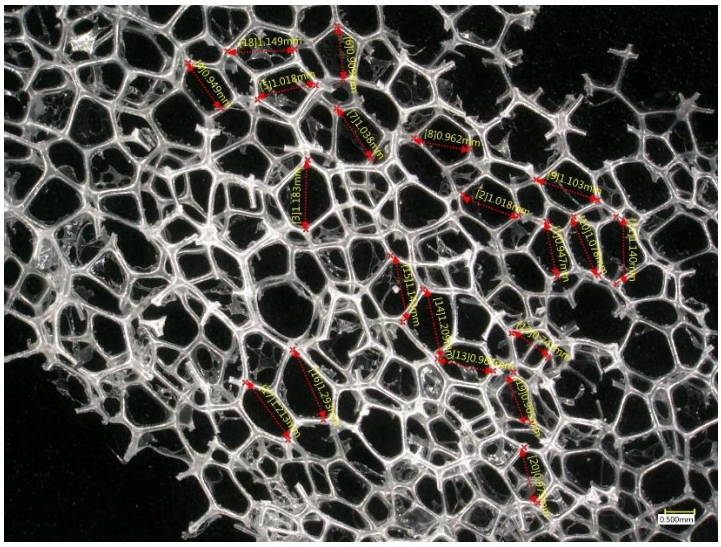

Figure 2.2: Light microscope image of a predominantly open-cell foam with overlaid pore measurements.

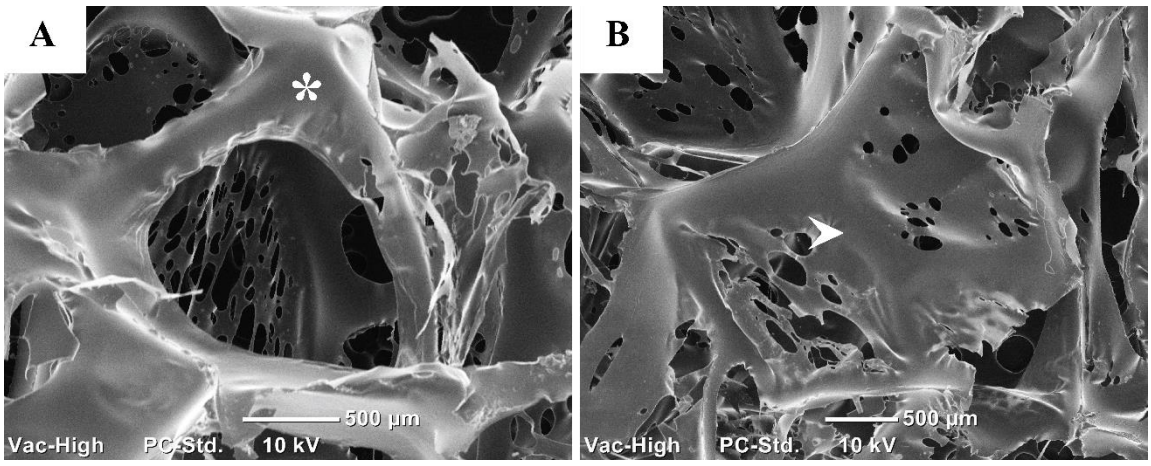

Figure 2.3: SEM images of H40 SMP foam with an (A) open-cell pore and a (B) partially close-cell pore. Asterisk indicates foam strut; Arrowhead indicates membrane. Synthesis of foam courtesy of Dr. Marziya Hasan, Alexa Easely, and Grace Fletcher.

Due to the foaming process thin residual membranes are observed between struts. The membranes form a predominantly closed cell structure, and can be removed by secondary physical processes such as hydrolysis, oxidation, heat, plasma etching, or

mechanical treatment [21, 22]. A closed cell microstructure may not be conducive for embolic materials as the lack of interconnected pores limit cellular infiltration during healing. Further, a closed cell microstructure may generate a large pressure gradient when deployed in the body, potentially causing the material to migrate after deployment [4, 21]. For these reasons mechanical reticulation was carried out, successfully resulting in a predominantly open-cell microstructure as shown in **Figures 2.2** and **Figure 2.3**.

Mechanical reticulation did not eliminate membranes entirely, but instead resulted in pseudo-open cell structures. **Figure 2.3B** shows a membrane that has micro-holes perforated through it. For the application of occluding a LAA the lack of completely open cells is not anticipated to be a major issue. Since the LAA is a terminal cavity with no downstream vasculature the danger of device migration downstream is non-existent, therefore a pressure gradient from a closed-cell structure is a low-risk situation. The key benefits of an open-cell microstructure for this application is rapid occlusion due to the formation of stable thrombus triggered by flow stagnation and recirculation through the interconnected foam matrix; as well as a cellular infiltration that improves the healing response [23, 24]. For this thesis, 0.008" nitinol wires punctured the membranes to provide a more open-cell structure. Despite incomplete removal of the membranes, 0.008" punctures are large enough to allow cells to infiltrate throughout the volume of the foam matrix.

Reticulation also affects the overall physical properties of the SMP foam. Blair et al. have reported reticulated foams have a decrease in the resistance to mechanical

compression [25]. Less resistance to compression may result in tighter crimping of the foam, thus decreasing the crimped diameter of the foam. A more compressed foam is beneficial to clinicians as it enables delivery through a low-profile catheter. A potential drawback of mechanical reticulation of foams is the potential for strut fracture and foam debris. It has been shown that reticulation results in significantly higher levels of particles when compared to a non-reticulated foam [26]. Within this thesis an approach to mitigate particle-release due to mechanical reticulation includes the encapsulation of the foam by a filter membrane.

2.3.2 Pore size

Eight foam batches were imaged in the transverse and axial directions, and were categorized as small (S), medium (M), or large (L) pore. **Table 2.3** summarizes the pore sizes of each foam batch, and their respective pore classification. Based on the results in **Table 2.3**, foams were cut in either the axial or transverse direction to achieve a suitable pore sizes. Anisotropic pore cells were also apparent from the difference in pore size between axial and transverse slices, which is typically seen in blown foams [27].

Table 2.3: Axial and transverse pore sizes of foam batches.

Pore Classification	Foam Batch	Axial Pore Size (μm)	Transverse Pore Size (μm)
Small (~1000 μm)	16011RCHAE01	1216 ± 189	906.6 ± 114
	160701RCHPEDGF06	1047 ± 133	1051 ± 228
	160525PEDAE01	1079 ± 135	813.9 ± 114/4
Medium (~1500 μm)	160511PEDMH02	1537 ± 186	1024.5 ± 121.7
	160515PEDAE03	1527.83 ± 252	1022.5 ± 173
	150913RCHMH04	1244.9 ± 245.1	1318.2 ± 175.15
	161004PEDAE01	1564 ± 300.5	1089.9 ± 195
Large (~1800 μm)	160929PEDAE01	1739.4 ± 359	927.8 ± 170

Pore size is believed to affect several key characteristics of foam performance. Landsman et al. performed mechanical analysis on several pore sizes and reported that foams with smaller pore sizes exert a greater radial force due to increased foam density [3]. Radial force is clinically significant as too low of a radial force poses a risk of the foam migrating, whereas a high radial force poses a risk of bursting or perforating the vessel. Fortunately, vessel rupture from high radial force is not a realistic risk of the present foam compositions considering Landsman et al. oversized similar foams by 50% to the target vessel and reported a radial force significantly lower than the required rupture force [3]. Device migration due to low radial force is a concern, however. To mitigate the risk of the foams migrating out of the LAA a nitinol frame may anchor the foam to the vessel wall. The WATCHMAN LAA closure device by Boston Scientific prevents device migration by incorporating metal anchors that engage surrounding tissue, in addition to the radial outward force from their nitinol cage [28].

Pore size, and thus foam density, also affects expansion rates. Smaller pore sizes, or higher foam density, delays water from penetrating and plasticizing the foam [3]. As a result, foam may not expand as fast when compared to larger pore foam.

2.3.3 Thermal properties

DSC was used to characterize the thermal properties of the thermoset SMP foams in wet and dry environments. In particular, the transition temperature at which foams undergo shape change corresponds to the T_g. **Table 2.4** shows that the average dry T_g of all investigated foams was between 59°C and 64°C with a max deviation of ± 2.4°C. Based on the dry T_g results the foams may be stored at room temperature if the surrounding environment is dry. The wet T_g was between 13 and 16°C, indicating that the foam will undergo shape change when placed into the body.

Pore size did not have a significant effect on the transition temperatures of the foam. This is expected as the foams were all of the same composition (i.e. H40). By varying the ratio of HPED to TEA in the foam formulation the transition temperatures can be precisely controlled. It is believed that the secondary hydroxyl group within HPED can present steric hinderance to rotational motion around the urethane linkage, and HPED can provide a higher crosslink density in comparison to TEA; thus increasing the T_g [22]. Landsman et al. supported that logic by showing that an H20 composition had a T_g 20°C less than the higher HPED content H60 composition [3].

Table 2.4: Wet and dry T_g temperatures for small, medium, and large pore foams.

Pore Size	Average Dry Tg (°C)	Std. Dev.	Average Wet Tg (°C)	Std. Dev.
Small Pore	59.53	1.45	13.52	1.84
Medium Pore	61.65	2.40	15.34	2.99
Large Pore	63.24	0.29	15.27	0.99

2.3.4 Expansion profiles

Characterizing the rate of expansion and final crimped diameter is critical to the performance of an embolization device. The crimped diameter regulates what size delivery catheter is suitable; typically, a lower-profile delivery catheter is desired as it can access more vasculature. The rate of expansion of SMP foam determines whether premature or delayed expansion will affect procedural outcomes. Premature expansion can cause the device to occlude the catheter, thus preventing deployment. Incomplete, or delayed expansion can result in incomplete occlusion of the vasculature, prolonged procedural times, or migration of the device.

Figure 2.4 shows the final crimped diameter of the foam as a function of bore diameter and pore size. Pore and bore size both had an effect on the final crimped diameter. In general, a trend depicting a decrease in crimped diameter as bore and pore size increased was observed. As bore and pore size increased the foam density decreased, thus allowing the foam to be crimped to smaller diameters.

A two-way analysis of variance (ANOVA) with Tuley post-hoc multiple comparison was conducted to examine the effect of pore size and bore size on crimped

diameter of SMP foam. Main effect analysis showed increasing pore and bore size significantly decreased crimped diameter. However, there was no significant interaction between pore and bore size. Tukey pairwise multiple comparison showed a significant difference between the majority of bore sizes when pore size was held constant. There was no significant difference between pore sizes, however. Two-way ANOVA was performed using Graphpad Prism 7 (Graphpad Software, Inc, La Jolla, CA).

Table 2.5 shows increasing bore and pore sizes increase the expansion ratio of foams, wherein the expansion ratio is defined as:

$$Expansion\ Ratio = \frac{30\ mm}{Crimped\ Diameter\ (mm)}$$

A max expansion ratio greater than 10 and a 61-fold volumetric expansion was recorded.

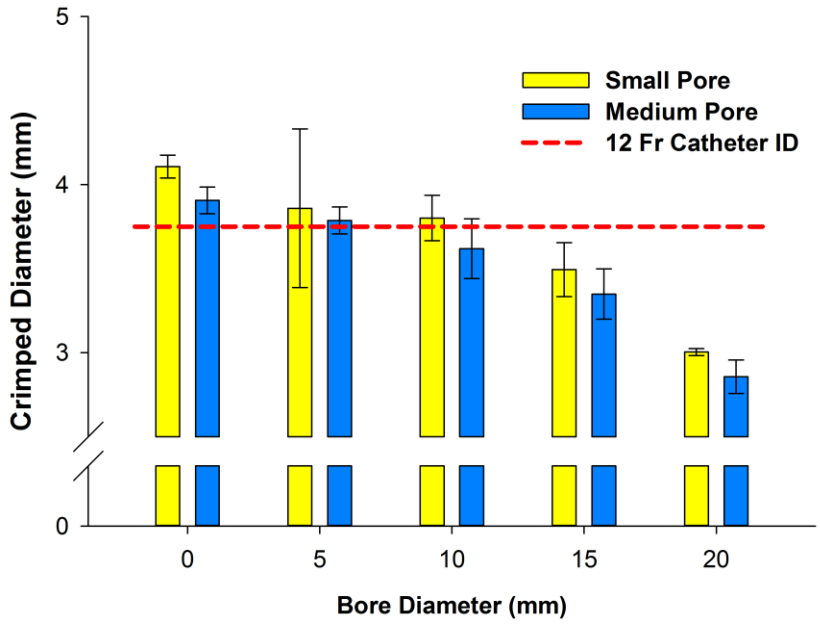

Figure 2.4: Final crimped diameter as a function of pore and bore diameter. The ID of a 12 Fr catheter is taken as 3.75 mm (N ≥ 3).

Table 2.5: The average expansion ratios ± standard deviation of H40 foams as a function of bore and pore size (N ≥ 3). N/A corresponds to insufficient data due to limited availability of foams.

Bore Size (mm)	Small Pore	Medium Pore	Large Pore
0	7.31 ± 0.12	7.68 ± 0.15	7.49 ± 0.01
5	7.85 ± 0.90	7.92 ± 0.20	7.73 ± 0.06
10	7.90 ± 0.31	8.30 ± 0.33	8.16 ± 0.22
15	8.60 ± 0.41	8.97 ± 0.17	N/A
20	9.99 ± 0.07	10.42 ± 0.19	N/A

The rate of expansion of SMP foams as a function of pore and bore diameter is shown in **Figure 2.5**. Most foams were able to expand to their original diameter in body-temperature water in under 10 minutes. To identify any trends in the data an index was selected for each data set and compared. The index was taken as the time it took the foam to expand to half its expanded diameter (Appendix D). No statistical or qualitative trend was observed.

Possible explanations for the lack of observable trends include: compromised mechanical properties due to boring of the foam that affected shape memory, irregular crimping, temperature fluctuations, or image analysis error.

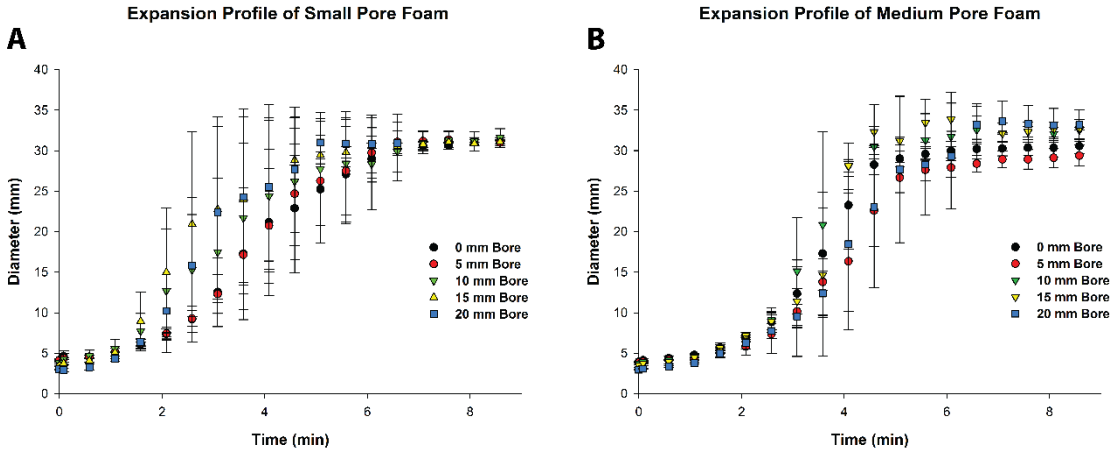

Figure 2.5: Expansion profiles as a function of pore and bore diameter.

A potential complication for passively-actuated embolization devices is premature expansion in the delivery catheter. To compound the risk, it is common practice to flush the delivery catheter containing the embolization device with saline to purge air and prevent air embolisms [28, 29]. To mitigate premature expansion of the foam the T_g may be tailored appropriately. Furthermore, the encapsulation of the SMP foam within a membrane or nitinol frame may be able to contain the foam enough to allow the clinician to deliver the device.

3. DESIGN AND FABRICATION OF A SHEATHED EMBOLIZATION DEVICE

3.1 Introduction

While SMP foam is a promising material for embolization devices, there exists a risk of unintended ischemia due to foam particulates entering the blood stream as emboli [26, 30]. This risk is compounded if SMP foam is in contact with nitinol mesh, wire, or other hard materials that can mechanically shear chunks of the low-density foam. Fabrication of a stand-alone device comprised of SMP foam and an emboli-capturing membrane may prevent foam based emboli from entering the bloodstream, and expand the commercial and clinical utility of SMP foams. A successful sheathed embolization device (SED) comprised of SMP foam could potentially be integrated with metals or predicate devices to improve the current standard of care for embolization procedures.

Additional concerns for developing a stand-alone SED include the mechanism of delivery and deployment, as well as imaging under fluoroscopy. Two popular LAAC devices, the WATCHMAN and Amplatzer Cardiac Plug (ACP, St. Jude Medical, Plymouth, Minnesota), are secured to a delivery cable and deployed by unscrewing the delivery cable [31, 32]. These devices are repositionable and retrievable. The WATCHMAN, and new versions of the ACP, come pre-loaded inside a delivery system and are deployed by holding the delivery cable fixed while slowly withdrawing the delivery catheter; as opposed to pushing the device [32, 33]. Fluoroscopic imaging is critical to proper device placement, and is achieved via marker bands on the delivery

system (i.e. access sheaths and delivery catheters) and from the inherent radiopacity of the nitinol that makes up the bulk of LAAC devices [14].

Within this chapter, a SED utilizing SMP foam as the main embolic material and a thin encapsulating membrane to provide emboli protection has been developed. The SED prototype also incorporates a delivery mechanisms that allows for fluoroscopic imaging to aid in device positioning. Within this chapter the material and design rationale will be provided, as well as the details for fabricating the SED. Lastly, components of the SED will be characterized to provide justification for their use, as well as insight to future improvements.

3.2 Design considerations

Designing a SED that takes into consideration the clinical utility, performance, safety, and manufacturing concerns can improve the quality of the final device. A thorough literature review and analysis of adverse events regarding embolization devices, particularly LAAC devices, delineated design criteria and requirements specified in **Table 3.1**.

Table 3.1: Design considerations for the development of SED.

Design Criteria	Design Requirement
Compatible with current delivery systems	Deliverable through a 12Fr catheter
Able to treat large LAA's	Expands to a diameter of 30 mm
Delivery mechanism	Simple and easy mechanism to delivery and deploy device
Radiopacity	Must be visible under fluoroscopy
Particulate reduction	A significant reduction in particulates between a sheathed and non-sheathed embolization device
Occlusion	Allows blood and cellular infiltration throughout the foam matrix
Wall apposition	Device should conform to the irregularly shaped LAA wall
Cost and ease of manufacturing	Devices should be assembled in a cost and time efficient manner
Integration with hard materials	The device should have potential to integrate with nitinol or predicate devices to expand the clinical and commercial utility
Ability to be recaptured	Should be retractable to be enticing to clinicians
Biocompatibility and hemocompatibility	Materials and device should: illicit a healing response, form an endothelial layer, and not form an unstable, undesired thrombus

3.3 Device fabrication

3.3.1 Summary of device design and fabrication

A SED design consisting of a SMP foam occlusion member, emboli-capturing membrane, and delivery system is shown in **Figure 3.1** and **Figure 3.3**. The overall device geometry is a cylinder that is roughly 2 cm long and 3 cm in diameter in order to occlude a large LAA. A membrane will fully encapsulate the SMP foam to capture as much foam particulates as possible. The ends of the device will have marker bands to aid in device imaging, considering SMP foams not loaded with radiopaque filler have limited radiopacity [34, 35]. Lastly, a simple screw detachment mechanism will allow the clinician to deploy the device once positioned.

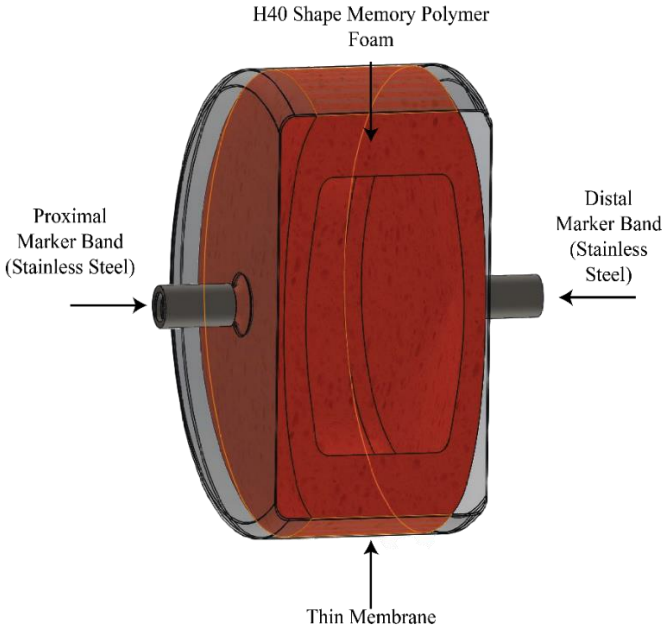

Figure 3.1: SED design concept.

3.3.2 Membrane selection

Several membranes were investigated for their use in developing a SED. Common materials used in cardiovascular applications include polytetrafluoroethylene (PTFE), polyethylene terephthalate (PET), and polyurethane (PU) (**Table 3.2**). PTFE, PET, and polyurethane films were investigated in this project due to their history in vascular applications and availability.

Table 3.2. Common medical fibers and biotextiles used in cardiovascular applications. Adapted from [36-38]. Abbreviations PTFE: Polytetrafluoroethylene; FEP: Fluorinated ethylene propylene polymer; ePTFE: Expanded polytetrafluoroethylene; PET: Polyethylene terephthalate; UHMWPE: Ultra high molecular weight polyethylene

Polymer Membrane	Mesh Pore Size (µm)	Cardiovascular Application
Polyester	30	Blood filter (ex vivo) [36, 39] Cardiac support device, Left atrial appendage closure device, Endovascular stent-graft, Vascular Prosthesis [36]
PTFE	N/A	Embolic vena cava filter, Endovascular stent-graft, Vascular Prosthesis, Left atrial appendage closure device [36]
FEP	N/A	Embolic vena cava filter [36]
UHMWPE	N/A	Left atrial appendage closure device [36]
Polyurethane	80 – 140	Embolic protection device [36, 40, 41]
PET	160 - 1016	Left atrial appendage closure devices [14, 37]
ePTFE	N/A	Left atrial appendage closure devices [14, 37]
Poly(carbonate)	N/A	Left atrial appendage closure devices [14, 37]
Nylon	N/A	Left atrial appendage closure devices [14, 37]

Ultimately, thermoplastic polyurethane (TPU) films were chosen to serve as the membrane to protect SMP foam from shear forces while filtering emboli. **Table 3.3** shows a comparison between the investigated materials. Common issues with the membrane materials included: its thickness, lack of elasticity, and its difficulty to process into cylinders.

Table 3.3: Comparison of investigated membrane materials.

Membrane Material	Thickness (µm)	Cost per device ($)	Processing Ability	Pore Size (µm)	Use in 510(k) submissions (or medical grade)
TPU films	23 – 28	~0.01	✓	Non-porous	Yes
PET	40 – 140	0.44	✓	40	No
UHMWPE	127 - 254	0.18	×	Non-porous	No
PTFE	127 - 254	0.36	×	Non-porous	No
ePTFE	10 - 1140	N/A	×	Non-porous	Yes

3.3.3 Thermoforming

Membranes should take the form of the body-cavity they are deployed in. Should membranes not be formed properly, and take on a non-ideal geometry, the SED may not expand properly to fully occlude the body-cavity. Thermoforming was considered as a method to shape and process plastic membranes. Stock membrane materials were typically delivered in a roll or as flat sheets, and needed to be processed to a shape that can house foam. Thermoforming is a secondary forming process that allows users to shape plastic in a softened, but still solid, thermoplastic state; unlike primary forming processes that occurs when the thermoplastic is a melt state [42]. Mechanical thermoforming typically involves clamping the plastic film in a positive or negative mold, then heating the plastic above its T_g or near its melting point depending if its amorphous or semi-crystalline, respectively. After the plastic is deformed or stretched over the mold it is cooled below its softening range to freeze its three-dimensional shape.

A fixture consisting of female mold and male former was designed in SolidWorks (Dassaut Systemes, Waltham, MA) that would shape the plastic membranes into a closed-end cylinder geometry (**Figure 3.2**). An aluminum fixture was machined via CNC according to the design. Membranes were wrapped around the male former, placed into the female mold, clamped, and then placed into a furnace. Depending on the thermal properties of the membrane material, the membrane was shaped into a closed-end cylinder similar to a tea-bag, and the excess material trimmed off.

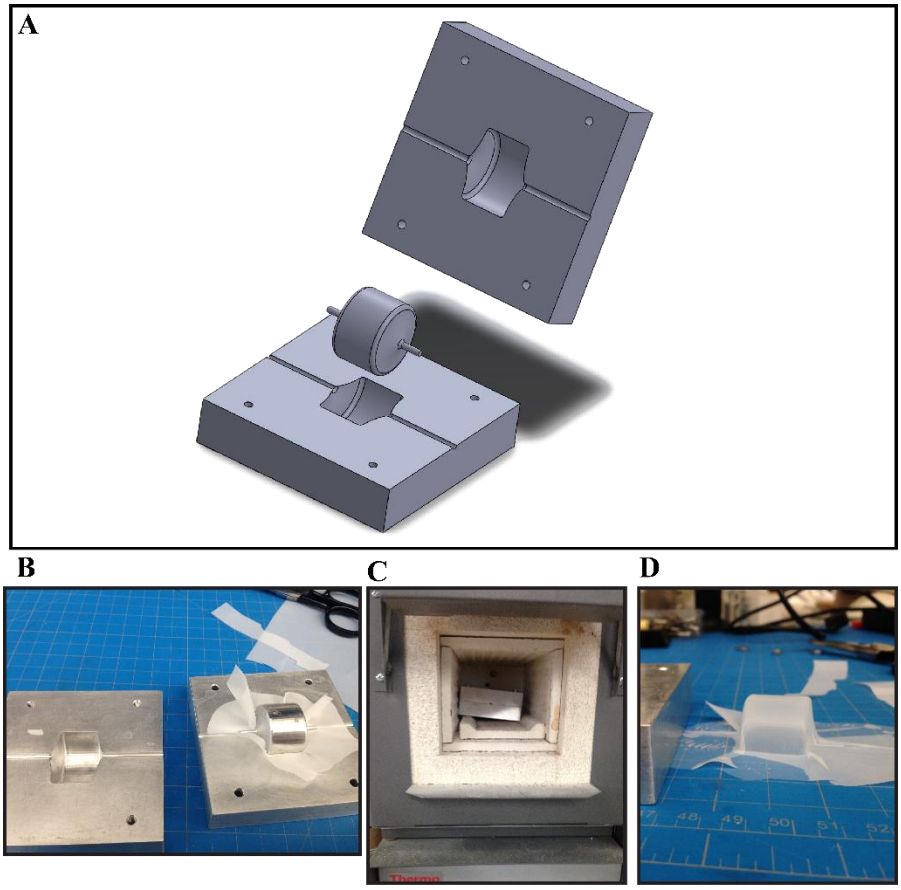

Figure 3.2: Processing membranes to take on a desired geometry via thermoforming. (A) SolidWorks design of fixture to mechanically thermoform plastic membranes. (B) Placement of membranes into fixture. (C) Placement of fixture into furnace. (D) Fixed three-dimensional membrane as a result of thermoforming.

3.3.4 Heat sealing

Heat sealing was the preferred method to seal the membrane of the SED. Two heat sealing methods were investigated. The first method consisted of using a solder iron that was heated to the membranes melting point, then applying a constant force along the areas to be sealed. However, this method was extremely unreliable as the contact force and temperature were difficult to control. The second method was to place the membrane into

fixture, clamp the sealing areas, and place into a furnace. This was achieved by wrapping the membrane around the foam and then carefully placing it into the fixture shown in **Figure 3.2**. The clamped fixture was then placed into a furnace for a set time and temperature, removed, and allowed to cool back to room temperature. The seams of the membrane that were clamped were sealed together, while the rest of the membrane and foam were not thermally damaged. The result was a fully encapsulated foam. Excess membrane material was trimmed with scissors or laser.

3.3.5 Membrane pore creation

A Gravograph LS100 40W CO_2 laser (Gravotech Inc., Duluth, GA) was used to cut pores into membrane materials. To do this, computer-aided design (CAD) software was used to make a 2-D pattern of pores and then exported to the laser-cutter software. The power and speed settings were set to 1% and 100%, respectively, for TPU films. The resolution was set to 1200 DPI.

3.3.6 Detachment mechanism and marker bands

A simple detachment mechanism serves to deploy, reposition, and release the device from a delivery catheter. Similar devices use a threaded release from the delivery cable or an interlocking release wire for controlled release of embolic materials [43]. In this thesis a simple threaded release system was fabricated (**Figure 3.3**). Stainless steel (SS) was used to fabricate the detachment system due to affordability, availability, and its radiopaque properties. SS is a radiopaque material, allowing it to be imaged during

interventional procedures [44]. Placement of the SS tubes on the ends of the SED may serve as marker bands for the clinician to position the device properly.

Stainless steel (SS) tubes (0.115-0.125” OD) were internally threaded (#4-40 or #0-80). These SS tubes were then epoxied to the ends of the SED to serve as marker bands, as well as to interface with the delivery cable. The delivery cable consisted of a torque cable that had a SS tube laser welded onto its distal end using an iWeld 990 (LaserStar, Riverside, RI). Filler wire and/or SS spacers were used to achieve a stable weld between the delivery cable and SS tube. A threaded SS rod was laser-welded at the distal end of the delivery cable/SS tube assembly, and interfaced with the SS marker bands on the SED. By simply twisting the delivery cable at the proximal end, a clinician may release the SED.

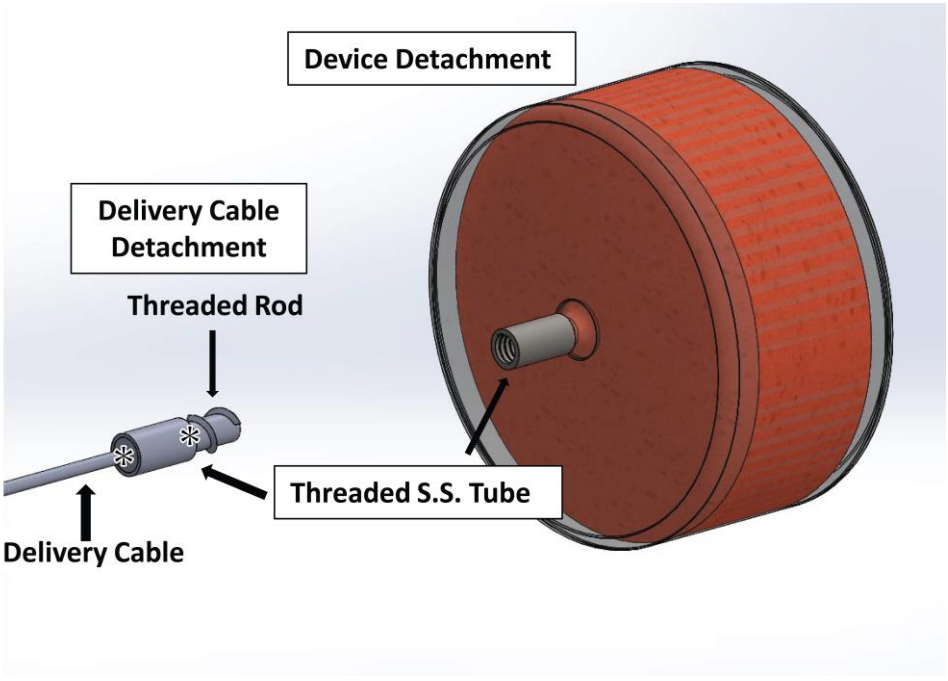

Figure 3.3: Delivery detachment components. Asterisks indicate laser welds.

3.4 Device characterization

3.4.1 Final device composition and fabrication

The final device composition is summarized in **Table 3.4** and shown in **Figure 3.4**. Detailed descriptions of the device's composition can be found in the following subsections.

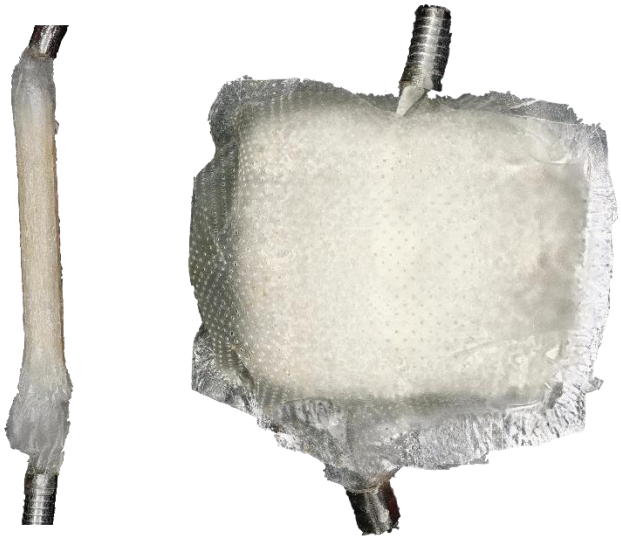

Figure 3.4: A crimped SED (left) and an expanded SED (right).

Table 3.4: Summary of final device composition.

Device component	**Component Description**
Occlusion Member	H40 SMP foam
Membrane	Porous TPU films (pore diameter = 261 μm; 10.54% porosity; thickness < 30 μm)
Marker Bands	SS tubes (5 mm length; 2.92 mm OD) on the proximal and distal ends of device
Delivery Mechanism	Screw-release; a threaded delivery cable interfaces with threaded marker bands on the device
Delivery Cable	A generic SS torque cable

The steps to fabricate and assemble a SED is shown in **Figure 3.5**. Briefly, a thin thermoplastic film is wrapped around a foam. The wrapped foam is then placed into an aluminum fixture. The aluminum fixture is then clamped together and placed into a furnace that is near the melting point of the film. While in the furnace, the film edges are heat sealed together. The fixture is then removed from the furnace and allowed to cool to room temperature. The fixture is then opened and the excess film is then trimmed or removed by laser. The wrapped foam is then removed and the ends are crimped. Stainless steel (SS) marker bands are then placed over the crimped ends and epoxied.

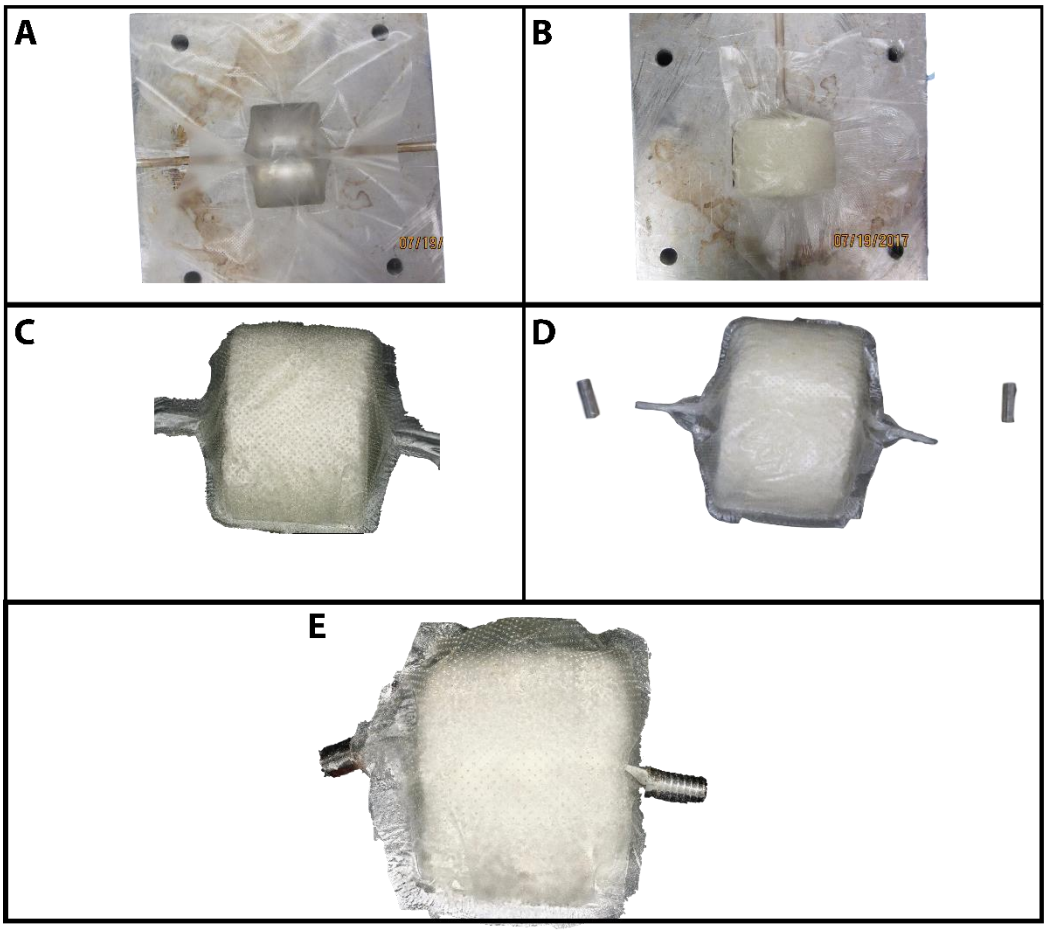

Figure 3.5: Fabrication of a SED. (A, B) A thin thermoplastic film and foam is placed into an aluminum fixture. The fixture is then placed into a furnace to heat seal the film together. (C) The edges of the film are trimmed by laser or razor. (D) The ends of the film are crimped to easily attach and epoxy SS marker bands. (E) The fully encapsulated foam with SS marker bands.

3.4.2 Membrane characterization

Thermoplastic polyurethane (TPU) films (AU25, EU28, and EU29; SWM International Inc., Alpharetta, GA) were chosen as membrane materials to encapsulate the SMP foam. These materials demonstrated the ability to undergo compression and expansion alongside the SMP foam. Furthermore, improved crimped diameters were achieved due to the material's thickness and elasticity. Within this section, the

morphology, thermal, and chemical properties of the TPU films were investigated. Other properties of the TPU film used in this thesis can be found in Appendix A.

TPU film surfaces were imaged as received with SEM following the same protocol in 2.2.4. A monolithic surface, as described by the manufacturer, with textured regions was observed **(Figure 3.6**). The textured regions, some of which appear to have pores, are most likely a result of rough handling. Despite being non-porous and a water barrier, the TPU films are breathable since they allow transmission of water vapor and have applications as wound dressings [45]. TPU films were laser-cut to create pores, as passage of blood and cells is critical to the performance of this application.

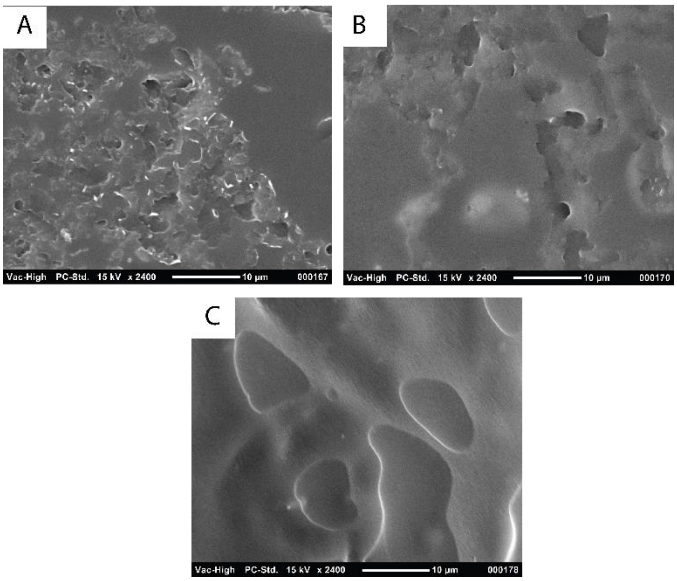

Figure 3.6: SEM images of (A) AU25 (B) EU28 and (C) EU29 TPU films at x2400 magnification.

Smooth concentric pores with a diameter of 261 ± 21 µm were created with a CO2 laser (**Figure 3.7**). Evidence of laser-induced melting was observed along the pore edges.

The pores are large enough to allow blood and cellular infiltrations, while being able to capture macro particulates. The theoretical porosity of the membrane was 10.54%, and was calculated by the following equation:

$$Porosity = Volume_{pore}/Volume_{film}$$

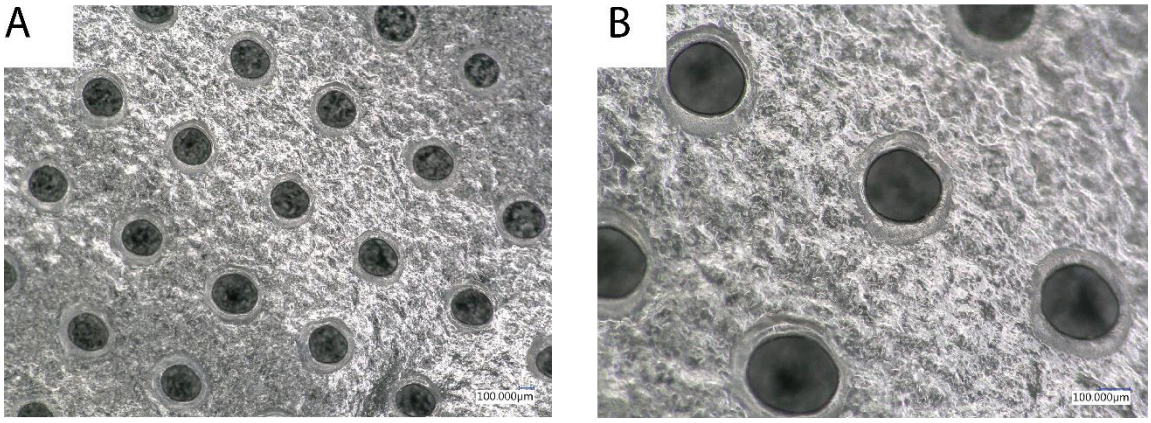

Figure 3.7: Light microscope images of laser created pores in TPU film; (A) 100x magnification (B) 200x magnification.

ATR-FTIR was performed, compliments of Dr. Mary Beth Browning Monroe, on the TPU films as received and neat H40 samples (**Figure 3.8**). The H40 neat samples refer to a non-blown, non-porous plastic that is compositionally identical the H40 foams. ATR FTIR spectra were obtained using a Bruker ALPHA Infrared Spectrometer (Bruker, Billerica, MA) with a diamond ATR crystal and analyzed with OPUS software (Bruker, Billerica, MA). Thirty-two background scans of the empty chamber were taken followed by sixty-four sample scans in absorption mode at a resolution of 4 cm^{-1}.

ATR FTIR confirmed the presence of urethane peaks at 1689 cm^{1} for the H40 neat film, as well as the TPU films. A strong C=O peak was observed for all plastics and

suggests hydrogen bonded urethane, which is characteristics of polyurethane polymers [22, 46]. A urea shoulder at ≈1647 cm^1 was present in the H40 composition due to the reaction of isocyanates with water during synthesis. A urea shoulder is expected in H40 foams as water is the chemical blowing agent used in traditional polyurethane foaming.

EU28 and EU29 TPU films had a shoulder at ≈1730 cm^{-1} due to the presence of polyesters [47]. Polyester polyurethanes have been reported to undergo rapid hydrolysis when implanted into the body, whereas polyether polyurethanes degrade via oxidation [48, 49]. A membrane that degrades into non-toxic byproducts following endothelialization would be ideal. AU25 TPU films lacked a 1730 cm^{-1} shoulder and is a polyether polyurethane.

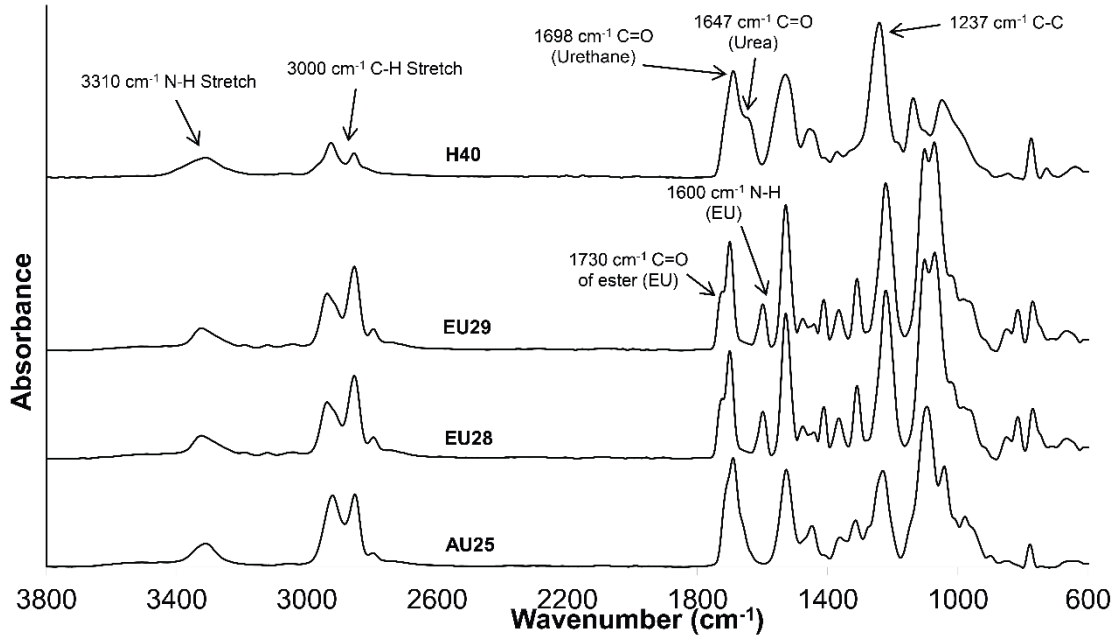

Figure 3.8: ATR FTIR spectra of H40 neat films and AU25, EU28, and EU29 TPU films.

Figure 3.9 shows DSC thermograms of the films. TPU samples (3-10 mg; N = 1) received as were hermetically sealed in aluminum pans. The DSC protocol specified an initial sample cooling to -80°C at a rate of 10°C/min, then holding it isothermally for 2 min. After the initial cooling, a heat ramp at a rate 10°C/min to 180°C proceeded and the sample was then cooled back to -80°C at the same rate. This cycle was repeated twice. T_g results did not change between cycles; but suspected melting points were erased on the following the first cycle.

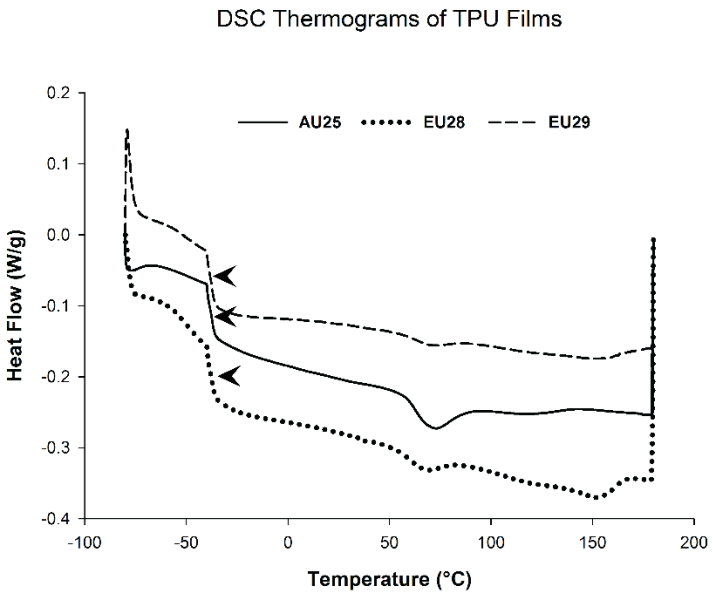

Figure 3.9: DSC thermograms showing the first heating cycle. Arrowheads indicate location of T_g.

Since the T_g of the TPU films is below freezing (-35 to -38°C), these materials are in their rubbery state under in-vivo conditions. Due to their low T_g temperatures, these films are not able to be thermoformed and do not hold a fixed shape at room or body temperature. As a result, these materials need to be expanded either by SMP foam, nitinol,

or balloons in vivo. Fortunately, the TPU films were soft and flexible enough to be expanded by SMP foam used in this thesis. A drawback of the thermal properties of these TPU films is that they do not hold their crimped geometry very well. In other words, once these TPU films are crimped over SMP foam they will relax; potentially clogging up the delivery catheter.

An ideal membrane would have a T_g at, or near body temperature. This would allow the membrane to retain its crimped geometry under storage conditions (i.e. room temperature with low humidity), while being able to expand under in-vivo conditions. More information is provided in chapter 5.

3.4.3 Delivery system

A generic torque cable was screwed into the marker bands of the SED. SS threaded rods and tubes were welded to the torque cable to enable screw detachment. Two screws (#0-80 and #4-40) were used to detach devices. The smaller screw, #0-80, performed better since it required less effort to detach the device. Occasionally, difficulty was noted when detaching the device. This can be attributed to poor laser-welds, improper threading, improper device placement, and a damaged torque cable.

4. TESTING OF A SHEATHED EMBOLIZATION DEVICE

4.1 Materials and methods

4.1.1 SED expansion

SEDs were fabricated from medium pore SMP foams and encapsulated with TPU films. The devices were threaded over 0.008" nitinol wire. The devices were crimped in a SC250 Stent Crimper that had a crimping pressure of 80 PSI at 80°C. The SEDs did not have a porous membrane and did not have SS marker bands epoxied to their ends. The crimped diameters of the SEDs were then recorded after 24 hours with calipers.

4.1.2 Bovine blood interaction

Bovine blood was acquired from the Rosenthal Meat Science and Technology Center (Texas A&M University, College Station, TX) as part of a tissue share program. The blood used in this study was collected from animals euthanized for purposes unrelated to this research. The blood was citrated in a 3.2% sodium citrate solution to prevent clotting, and stored at 4°C until use.

Several SEDs were prepared to investigate how bovine blood affects their performance. **Table 4.1** summarizes the SEDs used in this study. The SMP foams used in all SEDs were non-cleaned, non-reticulated H40 foams. No marker bands were attached to the ends of the SEDs. Each SED was crimped and their dry weight recorded prior to the studies. Polypropylene containers were rinsed with PBS (0.1 M; 7.4 pH) and filled with

50 mL of bovine blood. The containers were then placed into a water bath to reach a temperature of 37.5°C ± 0.5°C.

Table 4.1: Description of SED samples used in the bovine blood study.

SED Description	Dry Weight (g)	Membrane	Type of Blood	ACT (s)
Non-porous SED	0.486	Non-porous TPU film	Activated	161
Porous SED	0.502	Porous TPU film	Activated	122
Non-porous SED	0.488	Non-porous TPU film	Citrated	>1500
Porous SED	0.498	Porous TPU film	Citrated	>1500

Activated blood was used for some samples. To activate the blood 105 μL of 0.1 M $CaCl_2$ was added to every mL of bovine blood to achieve an activated clotting time (ACT) of 120 – 180 s [3]. ACT was checked by adding 2 mL of blood into kaolin-activated test vials and inserting the vials into a Hemochron® 401 (International Technidyne Corporation, Edison, NJ, USA).

SEDs were rinsed in PBS immediately prior to incubation in the containers containing blood. SEDs were submerged in citrated blood for 1 hour, and 30 minutes in activated blood. The SEDs were then removed, rinsed gently with PBS to wash away non-adherent thrombus, imaged, and dried overnight in a 50°C oven. A control foam was placed in the oven alongside the clotted devices to ensure the devices were thoroughly dried. Once dried the SEDs were weighed to quantify the mass of clot/blood on the device. Devices were then imaged again, and prepared for SEM.

4.1.3 Delivery into an anatomical model

An anatomical model based on computed tomographic (CT) images of a human LAA was fabricated to test the SEDs. CT image data of a human heart was acquired through OsiriX image library [50]. The left atrium and LAA were then isolated utilizing image thresholding tools on the 3D Slicer platform developed by NIH (**Figure 4.1**) [51]. A surface mesh of the model was then created and further processed with MeshLab software [52]. The surface mesh was verified to ensure it was watertight and had a minimum wall thickness to enable 3D printing. Isolating the LAA from CT data and converting it to a mesh is shown in **Figure 4.1**.

The isolated left atrium and LAA mesh was then 3D printed. The 3D printed model was then vapor polished with acetone. The 3D printed model was then placed into a box with smooth walls, and had polydimethylsiloxane (PDMS) casted around it. The PDMS was allowed to cure in a pressure chamber overnight, followed by a final cure in an oven set at 50°C for an hour. The mold was then placed into a heated base bath to dissolve the printed material from the PDMS cast. The final result was a PDMS model in the shape of the desired vessel geometry.

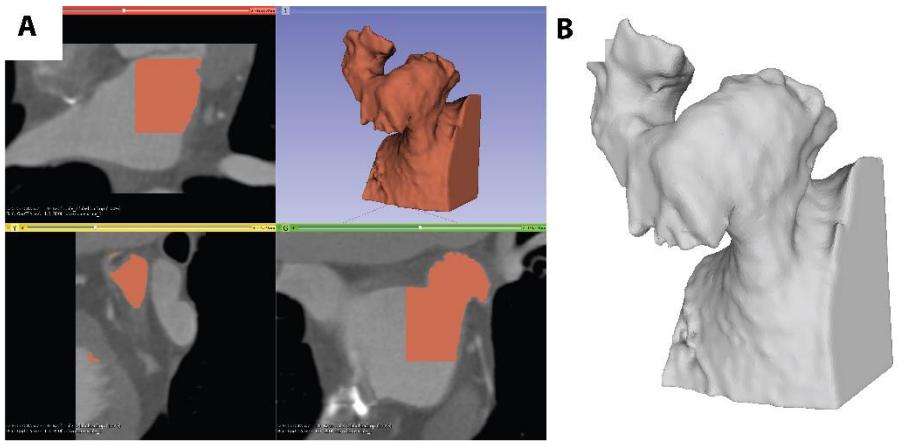

Figure 4.1: (A) Isolating target vessel geometry from CT data; (B) processed mesh suitable for 3D printing.

SEDs were pre-loaded in PTFE tubes and were delivered into anatomic models under minimal flow at body temperature. Devices were deployed in a similar manner described in Section 3.1. Once the devices were deployed and fully actuated the ability to recapture them was investigated. Additionally, the device detachment was investigated by unscrewing the delivery cable from the SEDs.

4.1.4 Device-ostium apposition

Fully actuated devices deployed within the anatomical models were imaged to quantify any gaps between the device and appendage ostium. To do this, a protocol described by Siewiorek et al. was used [40]. Briefly, the occluded models were positioned so the device and ostium were perpendicular to the camera's lens. Images were taken of the occluded model, along with a scale. The cross-sectional areas of the ostium and device were then measured with ImageJ. The device-ostium apposition was then quantified by taking the ratio of the ostium and device cross-sectional areas.

4.1.5 Particulate quantification

Particle counting by light microscopy was performed to quantify the particles generated by SMP foam, SEDs with a porous membrane, and SEDs with a non-porous membrane (N = 2). Mechanically-reticulated, non-cleaned SMP foams (30 mm OD; 20 mm length) were used as samples, and to fabricate SEDs. To improve visualization of the particles, foam was dyed following a protocol specified in Appendix E. The particle counting protocol used in this thesis was adapted from the USP 788 microscopic particle count test and is shown in **Figure 4.2** [15].

Briefly, samples were crimped and then placed into clean glassware containing 100 mL of particle-free water. The samples were then placed into a water bath set to 37°C for an hour under sonication to actuate the devices. The containers were then removed, inverted 20 times, and the contents passed through a cellulose filter under vacuum. The filter holder was then rinsed with 10 mL of particle-free water to re-suspend any particles adhering to the filter holder wall. Once the filter was free of water, the vacuum was stopped and the filter was carefully removed and placed onto a clean glass slide for further analysis.

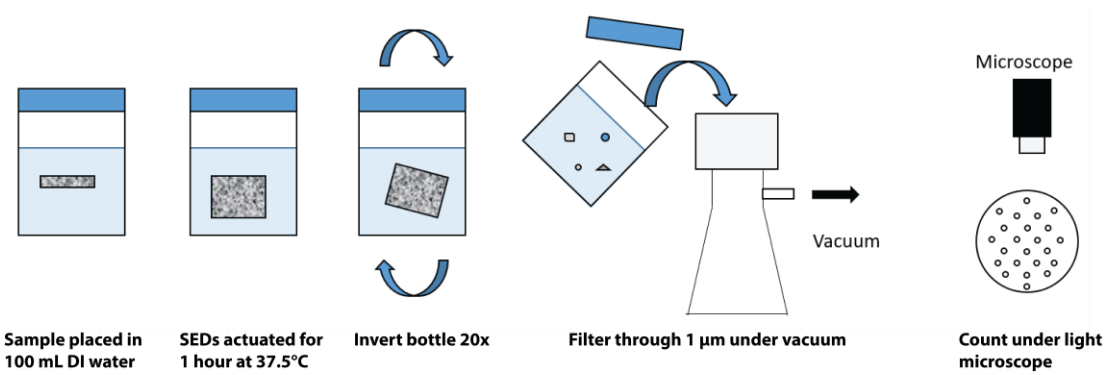

Figure 4.2: Schematic representation of the particle counting procedure.

Once the filter was dried, the filter was placed under a Keyence light microscope at a 100x magnification and examined. To count the particles, the Keyence systems "auto-measurement" software was used. The majority of the filter was analyzed by systematically moving the filter. Some filters were then analyzed under SEM by allowing them to dry at 80°C overnight, and sputter coating the surface of the filter with gold.

Results were compared to the acceptance criteria specified by USP 788 for small-volume (<100 mL) injections (**Table 4.2**). USP 788 identifies different acceptance criteria depending on the method of particle counting (e.g. light obscuration method vs microscopic particle count test).

Table 4.2: USP 788 acceptance criteria for injection or parenteral infusion for small volumes (< 100mL) [15].

Method	**≥ 10 µm**	**≥ 25 µm**
Light obscuration	6000	600
Microscopic particle count test	3000	300

To ensure the test environment did contribute significant amounts of particulate matter samples consisting of particle-free water were counted. The acceptable limits for a 100 mL sample of particle-free water are specified in **Table 4.3**. If the particle count is greater than the specified limits then the test environment is not suitable for particulate analysis.

Table 4.3: USP 788 limits for particle-free water per 100 mL sample [15].

Method	**≥ 10 µm**	**≥ 25 µm**
Light obscuration	100	20
Microscopic particle count test	40	10

4.2 Results

4.2.1 SED expansion

SEDs were capable of being crimped to fit within a 12 Fr catheter (ID ≤ 3.75 mm). By encapsulating the SMP foam within a TPU film the crimped diameter was increased, on average, by 0.42 ± 0.07 mm. The effect of bore size on crimped diameter is shown in **Figure 4.3**.

The crimped diameter reported in **Figure 4.3** includes the 0.008" nitinol wire threaded through the device, which was done to perform actuation studies. The crimped diameter is expected to decrease by 0.008" (0.20 mm) when fabricated without the nitinol wire. Actuation studies were performed on non-porous devices with an unestablished fabrication protocol, and therefore was omitted from this thesis. However, qualitative visual inspection of SEDs actuating during *in-vitro* studies resulted in full expansion in under 8 minutes (see section 4.2.4).

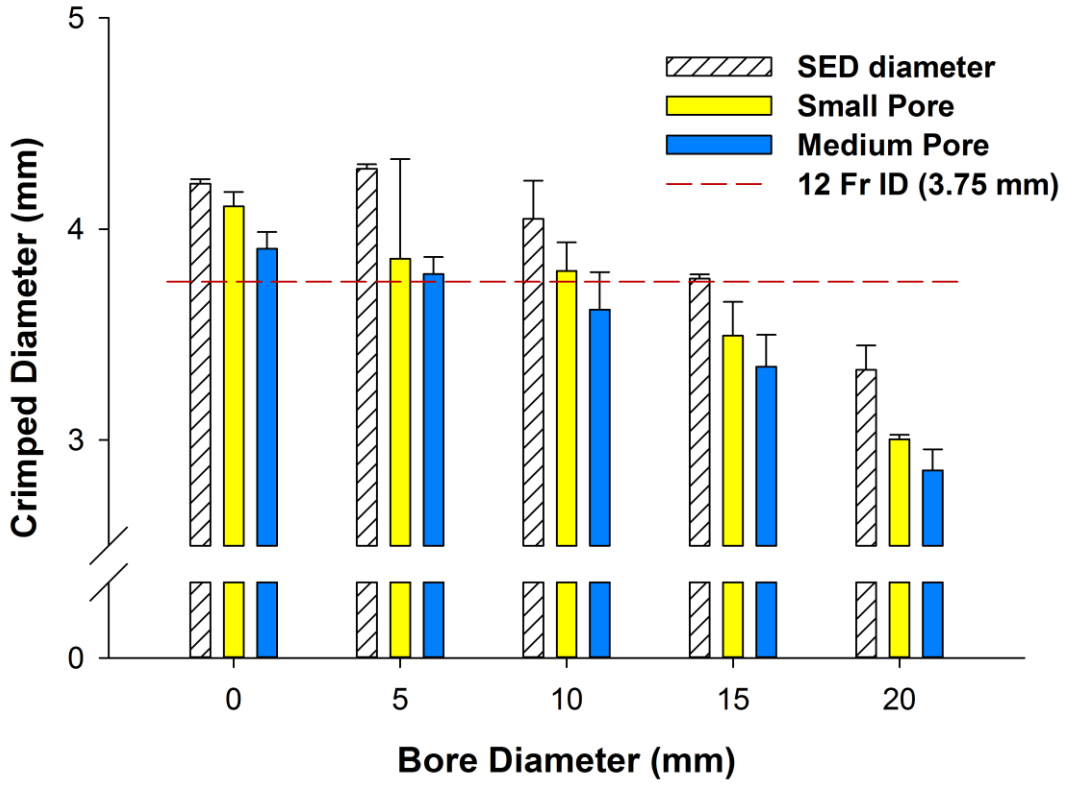

Figure 4.3: Crimped diameter of SEDs as a function of bore diameter. SEDs were fabricated with foams with medium sized pores, and crimped over a 0.008" nitinol wire (N = 2).

4.2.2 Device-blood interaction

Gravimetric analysis and qualitative images show SEDs were able to form clots and/or adsorb blood components. All devices were able to fully actuate when submerged in bovine blood, with the exception of a SED with a non-porous membrane that was submerged in activated bovine blood. The non-porous SED submerged in activated blood did not fully actuate because blood was not able to penetrate the device and depress the T_g before becoming clotted.

Thrombus formed in the gaps between SMP foam and the membrane (**Figure 4.4A**). This is beneficial as the additional thrombus may improve volumetric filling of the target vessel and prevent SMP particles from entering circulation. No blood clots formed on devices submerged in citrated blood. However, citrated blood was adsorbed throughout the entirety of the devices (**Figure 4.4C, D**). **Table 4.4** shows a major difference between the mass of clot formed on porous and non-porous SEDs. The mass of a control foam was recorded prior to submerging it in water and after drying it alongside clotted foams to verify all moisture was removed.

Table 4.4: Results of submerged SED samples in bovine blood (N = 1).

Sample Description	Blood Status	Initial Mass (g)	Dried Mass (g)	% Change
Non-porous SED	Activated	0.486	0.568	16.9
Porous SED	Activated	0.502	1.23	145
Non-porous SED	Citrated	0.488	1.31	168
Porous SED	Citrated	0.498	1.49	201
Control foam	N/A	0.420	0.410	-2.42

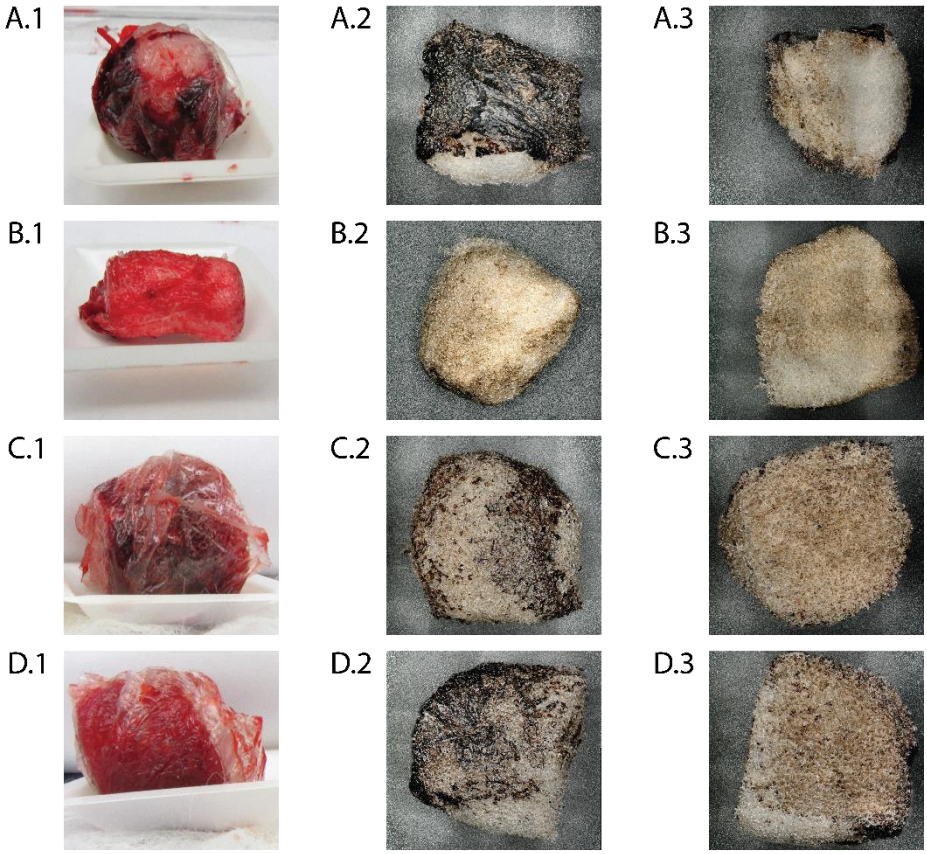

Figure 4.4: (A) SED with porous membrane submerged in activated bovine blood; (B) SED with non-porous membrane submerged in activated bovine blood; (C) SED with porous membrane submerged in citrated bovine blood; (D) SED with non-porous membrane submerged in citrated bovine blood. (A.1, B.1, C.1, D.1) Devices imaged immediately after removal from blood; (A.2, B.2, C.2, D.2) outer surface of devices imaged after drying; (A.3, B.3, C.3, D.3) cross-sectional images of devices after drying.

SEM analysis revealed signs of thrombus-related events on SMP foam and TPU films that were submerged in activated bovine blood (**Figure 4.5**). On both SMP foam and TPU film surfaces droplet-like formations appeared. These droplet-like formations are thought to be related to the oven-drying procedure. Additionally, what appears to be platelet clusters intertwined with fibrin is observed on the surfaces of both SMP foam and

TPU film. Kawasaki et al. show SEM images of platelets that have similar morphology to the platelet clusters observed in this study [53].

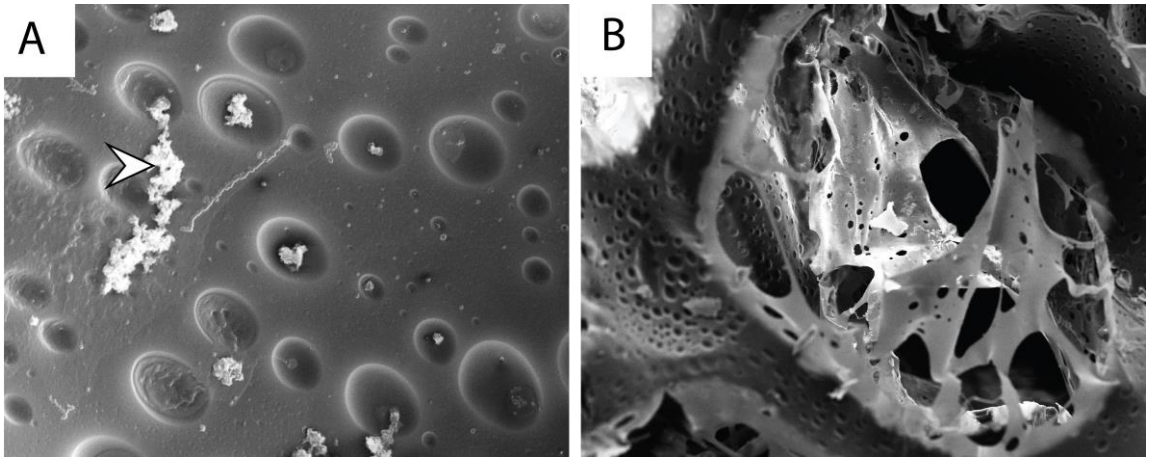

Figure 4.5: SEM images of thrombus-related materials on (A) TPU film and (B) SMP foam. Arrowhead indicates possible platelet cluster.

4.2.3 Device delivery

More than half of all the devices were delivered without complications and expanded to fill the ostium of the appendage in < 8 minutes (**Figure 4.6**). The majority of the complications were a result of insufficient radial force from the device to keep them fixed in the anatomic model. As a result, the device rotated with the detachment mechanism during deployment. Transitioning from a #4-40 to #0-80 screw improved the results, but ultimately the devices will have to be fixed in the anatomy to be practical. This can be achieved by incorporating nitinol, shape memory polymer, or coils to the device to anchor it to the vessel.

Unsheathing the device from the delivery catheter proved difficult at times. Parts of the device and delivery cable lacked column strength, and as a result the delivery cable would buckle or bend. Fortunately, switching to a stiffer delivery cable improved results.

Attempts to recapture fully expanded devices were unsuccessful. The devices were simply too large to fit inside the delivery catheter. Partial recapture (i.e. capturing half the device) was possible. Incorporating a metallic or polymeric frame around the devices may enable full recapturing in future device generations.

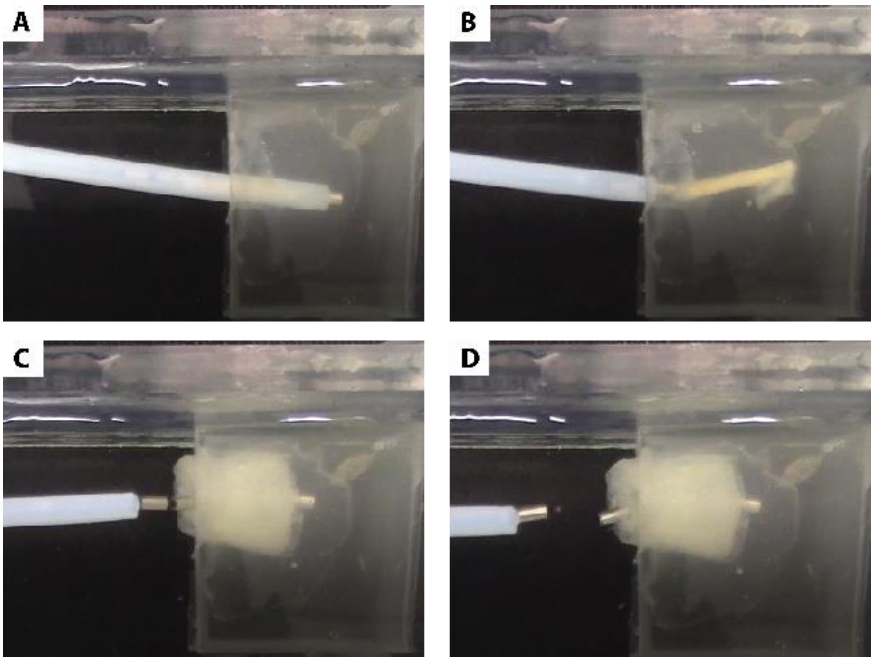

Figure 4.6: Benchtop delivery of SED. (A) A pre-loaded mock catheter is positioned into the LAA (B) the mock catheter is retracted while the SED and delivery cable are held in place (C) the SED is allowed to expand (D) the SED is detached from the delivery cable.

4.2.4 Device-ostium apposition

Gaps between the device and LAA ostium were quantified via image processing (**Figure 4.7**). All device geometries were able to occlude at least 86% of the ostium, with a majority of devices able to occlude roughly 95% of the ostium. Peri-device flow has been observed in roughly 32% of patients, and is considered to be insignificant if the leak is < 5 mm [54-57]. Ideally, there should be no gaps between the device and ostium in order to prevent any emboli from entering systemic circulation and to improve endothelialization.

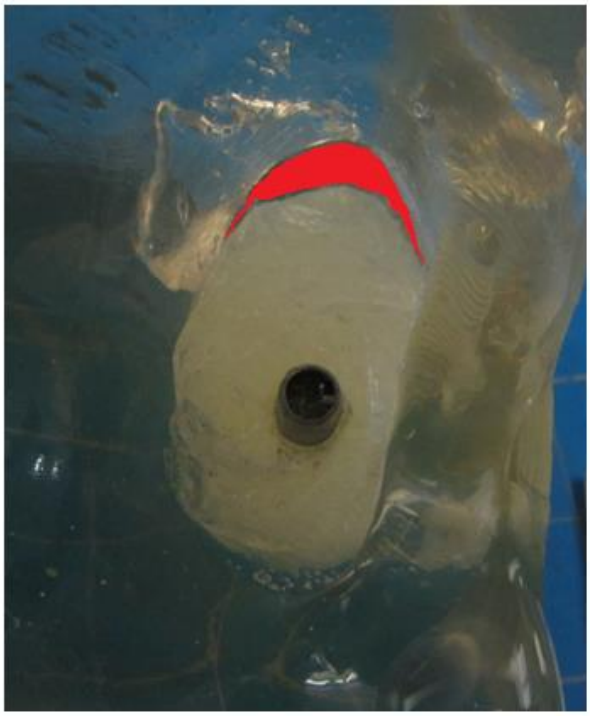

Figure 4.7: Device-ostium apposition of a 30 mm SED in benchtop model. The red indicates gaps between the device and the ostium.

Ostium geometry may limit the effectiveness of left atrial appendage closure devices. To determine if the benchtop models geometry was aggressively difficult when compared to clinical cases the "irregularity index" was calculated. The irregularity index correlates ostium geometry to residual leaks [58]. To calculate the irregularity index, the real and ideal area of the ostium are first recorded. The real area of the ostium is measured with any image processing software. The ideal area is calculated by measuring the major and minor axes of the ostium and using the following equation:

$$Ideal\ area = \pi \cdot major\ radius \cdot minor\ radius$$

The irregularity index is then calculated by the following equation:

$$Irregularity = abs[1 - (Ideal\ Area/Real\ Area)]$$

An irregularity index of 0.04 was identified as a threshold to predict a leak with a specificity of 94%. The irregularity index of the benchtop model in this study was around 0.027, which means the geometry of the benchtop model is not particularly irregular. In other words, the benchtop models geometry should be suitable for treatment. Since the SEDs did not completely seal the ostium, they may need to be more over-sized to conform to the ostium.

4.2.5 Particulate generation

The distribution of particles is shown in **Table 4.5** and **Figure 4.8**. The low amount of particles generated from particle-free water verifies the test environment is suitable for particulate analysis (limit ≥ 10 μm = 40, ≥ 25 μm = 10). A significant reduction in the number of particles was observed when SMP foam was encapsulated in a membrane. The

porous SEDs were compliant with the limits defined by the USP 788 light obscuration method (limit ≥ 10 μm = 6000, ≥ 25 μm = 600). However, the porous SEDs were not compliant with the limits defined by the USP 788 microscopic method, despite being close (limit ≥ 10 μm = 3000, ≥ 25 μm = 300). It is expected the devices would be compliant if they were cleaned and handled properly, and if the membrane pore size was decreased from 261 μm. Furthermore, the method of counting was performed with image analysis software that may have inflated the particle count.

Table 4.5: Mean ± standard deviation of particles counted for particles ≥ 10 μm and ≥ 25 μm.

Sample (N = 2)	≥ 10 μm	≥ 25 μm
Particle-free water	33.00 ± 8.485	8.500 ± 2.121
Foam	6057 ± 567.1	1805 ± 65.76
Porous SED	896.5 ± 129.4	372.0 ± 110.3
Non-porous SED	1934 ± 183.1	680.0 ± 306.9

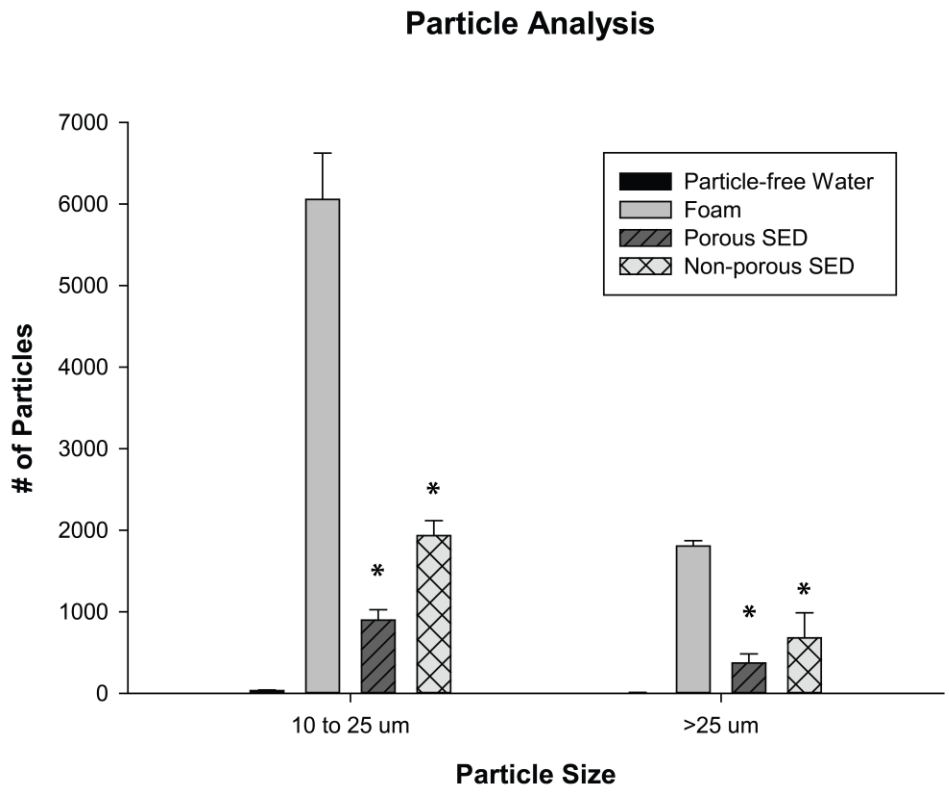

Figure 4.8: Number of particulates counted from particle-free water, SMP foam, a non-porous SED, and a porous SED. Asterisks indicate a significant difference ($p < 0.05$) when compared to SMP foam.

The main objective of this study was to compare the particle levels between a foam and a SED, and verify if there was a reduction of particles. **Figure 4.8** shows a significant reduction of particles between foam and devices, highlighting the utility of encapsulating foams. Interestingly, the non-porous SED samples generated more particles than the porous SED samples. This result was unexpected, considering the non-porous SEDs should not allow any encapsulated foam particles from escaping. Potential causes for the discrepancy include the handling of the samples and membrane tears. All samples were handled in ambient air and crimped in a non-sterile stent crimper that was not cleaned between samples. Furthermore, the non-porous SEDs were air-tight and could have burst

when crimped, similar to squeezing a balloon. The membrane was perforated with a needle a few times to prevent bursting, but could have been ineffective.

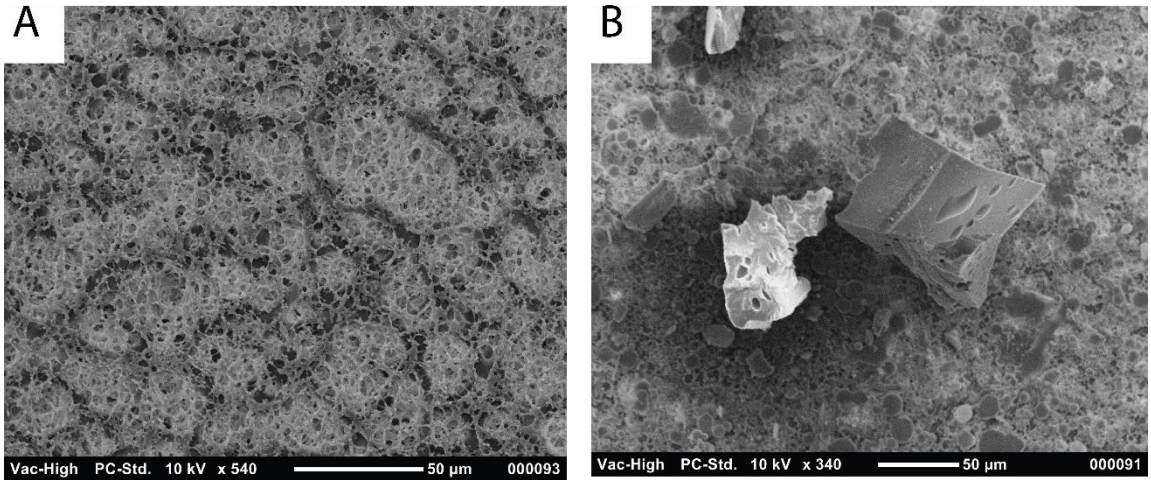

Figure 4.9: SEM images of (A) filter membrane and (B) particles on filter membrane.

Based on SEM and light microscopy images, the largest particles were fractured struts that were long but narrow. Numerous particles composed of thin SMP cell membranes were also observed (**Figure 4.9**). The SMP cell membranes were typically trapezoidal and came in many different sizes that were less than 200 µm. The amount of particles composed of cell membranes would be expected to drop if the SMP foam was reticulated and thoroughly washed [26].

Micro-embolization of cerebral arteries is an inherent risk for embolic protection devices and for the SEDs described in this thesis [59]. Matsuda et al. have reported stroke victims show pathological evidence of occluded arterioles ranging from 50 to 300 µm [60]. The danger of micro-embolization is further supported by a series of patients who developed neurologic dysfunction following a cardiac procedure. These patients died

shortly after and autopsy revealed acellular material (< 70 μm), believed to be emboli, deposited in their cerebral microvasculature [61]. Despite the risk of micro-embolization, the SEDs reduce the risk of macro and micro-embolization relative to a non-encapsulated SMP foam. A reduction of the SED's membrane pore size, in conjunction with improved filter design and proper cleaning, is expected to improve the capture of particles.

5. CONCLUSIONS AND FUTURE WORK

5.1 Summary

SMP foams have been used in endovascular applications due to their ability to volumetrically fill body cavities after being deployed via catheter. These foams, however, pose a risk of generating harmful particulates that can cause unintended ischemia. The risk of generating harmful particulates is further increased when SMP foam is in contact with nitinol, or other hard materials that are common in endovascular devices. The main objective of this thesis was, therefore, to mitigate the risk of SMP foams generating particulates. To do this a sheathed embolization device (SED) was designed, fabricated, and tested in the context of closing left atrial appendages (LAAs). Left atrial appendage closure (LAAC) was chosen as the intended application for the device because predicate devices are composed of nitinol, and if this device is successful could be integrated with predicate devices. Furthermore, LAAC is of great commercial and research interest in the Biomedical Device Lab.

In Chapter 2, the SMP foams used to develop SEDs were characterized. A main concern for the development of a SED for LAAC was determining a method to allow SMP foam to undergo a 10x diameter expansion. SMP foams were needed to expand to an OD of 30 mm following delivery from a 12 Fr catheter; which roughly corresponds to a 10x diameter expansion. To do this, cylindrical SMP foams were bored, or hollowed, in the center in an effort to increase the expansion ratios. Results showed that SMP foams were able to reach a 10x expansion when a 20 mm hole was punched through the center.

Increasing the pore size and bore size increased the expansion ratio of SMP foam due to the decrease in foam density. Regardless of pore or bore size, all SMP foams were able to expand to 30 mm or greater from a compressed state when placed in body temperature water.

Chapter 3 reviewed the design and fabrication of a SED. The final design chosen consisted of a SMP foam encapsulated in a porous TPU film that had stainless steel tubes epoxied to both ends. To deliver and deploy the SED, a simple screw-mechanism was designed and fabricated. TPU films were chemically, thermally, and morphologically characterized. ATR-FTIR confirmed the presence of polyurethane in the TPU films, and also revealed one of the films was a polyether-polyurethane film. DSC revealed the TPU films had a T_g below freezing. The low T_g allows the films to expand in tandem with SMP foam when placed into the body, however, it also means the films may not hold their crimped geometry. SEM analysis of the as-received TPU films revealed they were monolithic and impermeable to water. Thus, a CO_2 laser created uniform 261 μm pores into the TPU film to enable blood and cells to penetrate the SMP foam. The film was molded into a closed-end cylinder by placing wrapping it around foam and heat-sealing the ends. The stainless steel tubes epoxied to the ends of the device enable fluoroscopic imaging, and aid in delivering the device.

Chapter 4 tested the devices ability to be delivered via a 12 Fr catheter, occlude a LAA, reduce particles, and its ability to undergo actuation in blood and adsorb blood. Devices were capable of fitting within a 12 Fr catheter. Crimped devices were submerged into citrated and activated bovine blood and showed excellent actuation, suggesting that

under in-vivo conditions the device will actually expand to occlude the cavity. Devices also doubled their weight in adsorbed blood. Visual inspection revealed clotted bovine blood between the SMP foam and the TPU films, and that blood was able to penetrate deep within the foam. These results suggest that thrombus, in addition to SMP foam, may aid in occluding body cavities.

Devices were able to be successfully delivered into an anatomical model. Several observations were made that could improve device delivery including anchoring the device in the appendage, fabricating stiffer devices, and using a stiffer delivery cable. Gaps between the LAA ostium and devices were measured via image processing. Gaps between the device and ostium accounted for 4 to 14% of the ostium surface area.

A protocol based on USP 788 was adapted to count the number and size of particles that were generated as SMP foam actuated with or without a membrane. Results showed that encapsulating SMP foam in a TPU film significantly reduced the number of particles. SEM of the particles revealed troublesome particles composed of long and narrow foam struts, and thin cell membranes.

5.2 Challenges and future work

There were many limitations throughout the development of this thesis that I will briefly discuss in chronological order. To minimize the crimped diameter of the foam the centers were bored out. Sacrificing foam materials may inhibit healing, limit actuation, and reduce the radial expansion force of the foam. Limited actuation and radial expansion force could cause inadequate sealing and foam migration inside the body. Future studies

should include measuring the radial force of SEDs, and comparing the radial force to similar device. An alternative to boring out foam may be to increase the crimping pressure. However, the ability of water or blood to plasticize the foam may be restricted due to the tighter crimping pressure and affect expansion rates.

Finding a suitable material to encapsulate the SMP foam was the most difficult challenge of this thesis. Initially, PET (i.e. Dacron) was investigated because of its history in predicate devices. However, PET was a stiff, non-elastic material that would not expand from a crimped state. TPU films were then investigated and served their purpose but were still not the ideal material. As received TPU films were not porous, and did not retain their crimped geometry for extended periods of time. Furthermore, processing the TPU films to form porous cylinders resulted in seam-lines, rough edges, and large pores. Future work could include synthesizing porous SMP films with tailored transition temperatures. The SMP films could be thermoset or thermoplastic, but thermosets are expected to be much more difficult to process. Furthermore, work would need to be done to determine an optimal porosity. These films could even be surface-modified to be non-thrombogenic or loaded with drugs or growth factors.

Another significant challenge within this thesis included counting particles with light microscopy. For the most part, the USP 788 outlined protocol was strictly followed. However, upon analysis, the particles were difficult to differentiate from the filter background. To improve manual particle counting, black filter membranes may be used to improve the contrast against the white foam particles. Alternatively, foams may be dyed. Furthermore, manually counting the entirety of the filter is labor-intensive and not

practical. Fortunately, the microscope used in this study had built-in software to automate particle counting; though, it was never verified. The particle counting method should be verified by counting a known amount of calibrated particles, and ensuring a reasonable percentage of the calibrated particles are recovered.

Another challenge included delivering the devices under physiological conditions. In this thesis the devices were delivered into thick-walled PDMS anatomical models at body temperature with minimal flow. Ideally, the delivery would be performed under physiological conditions such as pulsatile flow with a blood-like fluid into an anatomical model that has similar mechanical characteristics of the natural anatomy. The delivery could even be performed under fluoroscopic guidance to verify the device can be positioned under clinical conditions. Lastly, the force to deliver devices through a catheter should be measured.

Following deployment of the SEDs in the benchtop model, it was observed the devices were not fixed and could easily migrate out of the appendage. To prevent device migration the devices should be augmented with super-elastic alloys or polymers, or coils. Furthermore, the force required to dislodge the devices once deployed in the model should be quantified.

A major motivation of this thesis was to reduce the generation of foam particles due to interaction with nitinol and hard materials. Future work would be to integrate SEDs with nitinol, and to repeat many of the tests outlined in this thesis.

REFERENCES

1. Horn, J., Hwang, W., Jessen, S.L., Keller, B.K., Miller, M.W., et al., *Comparison of shape memory polymer foam versus bare metal coil treatments in an in vivo porcine sidewall aneurysm model.* Journal of Biomedical Materials Research Part B: Applied Biomaterials, 2017. **105**(7): p. 1892-1905.

2. Hasan, S.M., Nash, L.D., and Maitland, D.J., *Porous shape memory polymers: Design and applications*. Journal of Polymer Science Part B: Polymer Physics, 2016. **54**(14): p. 1300-1318.

3. Landsman, T.L., Bush, R.L., Glowczwski, A., Horn, J., Jessen, S.L., et al., *Design and verification of a shape memory polymer peripheral occlusion device.* Journal of the Mechanical Behavior of Biomedical Materials, 2016. **63**: p. 195-206.

4. Rodriguez, J.N., Clubb, F.J., Wilson, T.S., Miller, M.W., Fossum, T.W., et al., *In vivo response to an implanted shape memory polyurethane foam in a porcine aneurysm model.* Journal of Biomedical Materials Research Part A, 2014. **102**(5): p. 1231-1242.

5. Romero, J., Cao, J.J., Garcia, M.J., and Taub, C.C., *Cardiac imaging for assessment of left atrial appendage stasis and thrombosis.* Nat Rev Cardiol, 2014. **11**(8): p. 470-480.

6. Holmes, D.R., Reddy, V.Y., Turi, Z.G., Doshi, S.K., Sievert, H., et al., *Percutaneous closure of the left atrial appendage versus warfarin therapy for prevention of stroke in patients with atrial fibrillation: a randomised non-inferiority trial.* The Lancet. **374**(9689): p. 534-542.

7. Lloyd-Jones, D.M., Wang, T.J., Leip, E.P., Larson, M.G., Levy, D., et al., *Lifetime risk for development of atrial fibrillation.* Circulation, 2004. **110**(9): p. 1042-1046.

8. Liverpool Heart and Chest Hospital. *Left Atrial Appendage Closure*. 2017; Available from: https://www.lhch.nhs.uk/media/4060/lefta-childsec.jpg.

9. Romero, J., Perez, I.E., Krumerman, A., Garcia, M.J., and Lucariello, R.J., *Left Atrial Appendage Closure Devices.* Clinical Medicine Insights. Cardiology, 2014. **8**: p. 45-52.

10. Akinapelli, A., Bansal, O., Chen, J.P., Pflugfelder, A., Gordon, N., et al., *Left Atrial Appendage Closure – The WATCHMAN Device.* Current Cardiology Reviews, 2015. **11**(4): p. 334-340.

11. Singh, I.M. and Holmes, D.R., *Left Atrial Appendage Closure.* Current Cardiology Reports, 2010. **12**(5): p. 413-421.

12. Lin, A.C. and Knight, B.P., *Left Atrial Appendage Closure.* Progress in Cardiovascular Diseases, 2015. **58**(2): p. 195-201.

13. Bergmann, M.W. and Landmesser, U., *Left atrial appendage closure for stroke prevention in non-valvular atrial fibrillation: rationale, devices in clinical development and insights into implantation techniques.* EuroIntervention, 2014. **10**(4): p. 497-504.

14. Saw, J. and Lempereur, M., *Percutaneous left atrial appendage closure: procedural techniques and outcomes.* JACC: Cardiovascular Interventions, 2014. **7**(11): p. 1205-1220.

15. Pharmacopeia, US,. *USP/NF General Chapter< 788>. Particulate matter in injections*. in *US Pharmacopeia, national formulary, USP35-NF-30. Rockville, Maryland: United States Pharmacopeial Convention*. 2012.

16. TIR42 AAMI, *Evaluation of particulates associated with vascular medical devices.* Association for the Advancement of Medical Instrumentation, 2010.

17. US Food Drug Administration, *Non-clinical engineering tests and recommended labeling for intravascular stents and associated delivery systems: guidance for industry and FDA staff. US Department of Health and Human Services.* Food and Drug Administration, Centre for Devices and Radiological, Health, 2010.

18. Kastrup, A., Gröschel, K., Krapf, H., Brehm, B.R., Dichgans, J., et al., *Early outcome of carotid angioplasty and stenting with and without cerebral protection devices.* Stroke, 2003. **34**(3): p. 813-819.

19. Hasan, S.M., Raymond, J.E., Wilson, T.S., Keller, B.K., and Maitland, D.J., *Effects of Isophorone Diisocyanate on the Thermal and Mechanical Properties of Shape-Memory Polyurethane Foams.* Macromolecular Chemistry and Physics, 2014. **215**(24): p. 2420-2429.

20. Rodriguez, J.N., Miller, M.W., Boyle, A., Horn, J., Yang, C.-K., et al., *Reticulation of low density shape memory polymer foam with an in vivo demonstration of vascular occlusion.* Journal of the Mechanical Behavior of Biomedical Materials, 2014. **40**: p. 102-114.

21. Nash, L.D., Docherty, N.C., Monroe, M.B.B., Ezell, K.P., Carrow, J.K., et al., *Cold plasma reticulation of shape memory embolic tissue scaffolds.* Macromolecular rapid communications, 2016. **37**(23): p. 1945-1951.

22. Singhal, P., Rodriguez, J.N., Small, W., Eagleston, S., Van de Water, J., et al., *Ultra Low Density and Highly Crosslinked Biocompatible Shape Memory Polyurethane Foams.* Journal of polymer science. Part B, Polymer physics, 2012. **50**(10): p. 724-737.

23. Small, W., Singhal, P., Wilson, T.S., and Maitland, D.J., *Biomedical applications of thermally activated shape memory polymers.* Journal of materials chemistry, 2010. **20**(18): p. 3356-3366.

24. Muschenborn, A.D., Ortega, J.M., Szafron, J.M., Szafron, D.J., and Maitland, D.J., *Porous media properties of reticulated shape memory polymer foams and mock embolic coils for aneurysm treatment.* BioMedical Engineering OnLine, 2013. **12**(1): p. 1-13.

25. Blair, E.A., *Cell structure: physical property relationships in elastomeric foams.* Cellular Plastics, Washington, 1967: p. 143-152.

26. Nathan, A.L., Fletcher, G.K., Monroe, M.B.B., Hwang, W., Herting, S.M., et al., *Particulate Release From Nanoparticle-Loaded Shape Memory Polymer Foams.* Journal of Medical Devices, 2017. **11**(1): p. 011009-011009-9.

27. Klempner, D. and Frisch, K.C., *Handbook of polymeric foams and foam technology*. Vol. 404. 1991: Hanser Munich etc.

28. Möbius-Winkler, S., Majunke, N., Sandri, M., Mangner, N., Linke, A., et al., *Percutaneous left atrial appendage closure: technical aspects and prevention of periprocedural complications with the watchman device.* World journal of cardiology, 2015. **7**(2): p. 65.

29. Swaans, M.J., Alipour, A., Rensing, B.J.W.M., Post, M.C., and Boersma, L.V.A., *Catheter Ablation in Combination With Left Atrial Appendage Closure for Atrial Fibrillation.* Journal of Visualized Experiments : JoVE, 2013(72): p. 3818.

30. Vaidya, S., Tozer, K.R., and Chen, J., *An Overview of Embolic Agents.* Seminars in Interventional Radiology, 2008. **25**(3): p. 204-215.

31. Rodés-Cabau, J., Champagne, J., and Bernier, M., *Transcatheter closure of the left atrial appendage: Initial experience with the amplatzer cardiac plug device.* Catheterization and Cardiovascular Interventions, 2010. **76**(2): p. 186-192.

32. Quizhpe, A.R., Cadavid, A.F., Córdova, M.A., Vintimilla, J., Ortega, C., et al., *Left Atrial Appendage Closure With the Watchman™ Device.* Revista Brasileira de Cardiologia Invasiva (English Edition), 2014. **22**(1): p. 56-63.

33. Freixa, X., Chan, J.L.K., Tzikas, A., Garceau, P., Basmadjian, A., et al., *The Amplatzer™ Cardiac Plug 2 for left atrial appendage occlusion: novel features and first-in-man experience.* EuroIntervention, 2013. **8**(9): p. 1094-1098.

34. Hasan, S.M., Harmon, G., Zhou, F., Raymond, J.E., Gustafson, T.P., et al., *Tungsten-loaded SMP foam nanocomposites with inherent radiopacity and tunable thermo-mechanical properties.* Polymers for Advanced Technologies, 2016. **27**(2): p. 195-203.

35. Rodriguez, J.N., Yu, Y.-J., Miller, M.W., Wilson, T.S., Hartman, J., et al., *Opacification of Shape Memory Polymer Foam Designed for Treatment of Intracranial Aneurysms.* Annals of Biomedical Engineering, 2012. **40**(4): p. 883-897.

36. Ratner, B.D., Hoffman, A.S., Schoen, F.J., and Lemons, J.E., *Biomaterials science: an introduction to materials in medicine*. 2004: Academic press.

37. Lesh, M.D. and van der Burg, E.J., *Method and device for left atrial appendage occlusion*. 2000, Google Patents.

38. Theobald, E., Randolph, J.R., Pavcnik, D., Keller, F., Shirley, B., et al., *Multi-stage occlusion devices*. 2015, Google Patents.

39. Win, K.N., Wang, S., and Ündar, A., *Microemboli Generation, Detection and Characterization During CPB Procedures in Neonates, Infants, and Small Children.* ASAIO Journal, 2008. **54**(5): p. 486-490.

40. Siewiorek, G.M., Eskandari, M.K., and Finol, E.A., *The Angioguard(™) embolic protection device.* Expert review of medical devices, 2008. **5**(3): p. 287-296.

41. Order, B.-M., Glass, C., Liess, C., Heller, M., and Müller-Hülsbeck, S., *Comparison of 4 Cerebral Protection Filters for Carotid Angioplasty: An in Vitro Experiment Focusing on Carotid Anatomy.* Journal of Endovascular Therapy, 2004. **11**(2): p. 211-218.

42. Truckenmüller, R., Giselbrecht, S., Rivron, N., Gottwald, E., Saile, V., et al., *Thermoforming of film-based biomedical microdevices.* Advanced materials, 2011. **23**(11): p. 1311-1329.

43. Hogan, D.F., Green, H.W., and Sanders, R.A., *Transcatheter closure of patent ductus arteriosus in a dog with a peripheral vascular occlusion device.* Journal of Veterinary Cardiology, 2006. **8**(2): p. 139-143.

44. Violaris, A.G., Ozaki, Y., and Serruys, P.W., *Endovascular stents: a 'break through technology', future challenges.* The International Journal of Cardiac Imaging, 1997. **13**(1): p. 03-13.

45. Wu, P., Jones, G., Shelley, C., and Woelfli, B., *Novel microporous films and their composites.* Journal of engineered fibers and fabrics, 2007. **2**(1).

46. Singhal, P., Boyle, A., Brooks, M.L., Infanger, S., Letts, S., et al., *Controlling the Actuation Rate of Low-Density Shape-Memory Polymer Foams in Water.* Macromolecular Chemistry and Physics, 2013. **214**(11): p. 1204-1214.

47. Chen, Y., Zhou, S., Yang, H., and Wu, L., *Structure and properties of polyurethane/nanosilica composites.* Journal of Applied Polymer Science, 2005. **95**(5): p. 1032-1039.

48. Marois, Y. and Guidoin, R., *Biocompatibility of polyurethanes.* 2013.

49. Davis, F.J. and Mitchell, G.R., *Polyurethane based materials with applications in medical devices.* Biomater Prototyping Appl Med, 2008. **3**: p. 27-48.

50. Rosset, A., Spadola, L., and Ratib, O., *OsiriX: an open-source software for navigating in multidimensional DICOM images.* Journal of digital imaging, 2004. **17**(3): p. 205-216.

51. Fedorov, A., Beichel, R., Kalpathy-Cramer, J., Finet, J., Fillion-Robin, J.-C., et al., *3D Slicer as an image computing platform for the Quantitative Imaging Network.* Magnetic resonance imaging, 2012. **30**(9): p. 1323-1341.

52. Cignoni, P., Corsini, M., and Ranzuglia, G., *Meshlab: an open-source 3d mesh processing system.* Ercim news, 2008. **73**(45-46): p. 6.

53. Kawasaki, J., Katori, N., Kodaka, M., Miyao, H., and Tanaka, K.A., *Electron microscopic evaluations of clot morphology during thrombelastography®.* Anesthesia & Analgesia, 2004. **99**(5): p. 1440-1444.

54. Akin, I. and Nienaber, C.A., *Left atrial appendage occlusion: A better alternative to anticoagulation?* World Journal of Cardiology, 2017. **9**(2): p. 139-146.

55. Chung, H., Jeon, B., Chang, H.-J., Han, D., Shim, H., et al., *Predicting Peri-Device Leakage of Left Atrial Appendage Device Closure Using Novel Three-Dimensional Geometric CT Analysis.* Journal of Cardiovascular Ultrasound, 2015. **23**(4): p. 211-218.

56. Kapur, S. and Mansour, M., *Left Atrial Appendage Closure Devices For Stroke Prevention.* Arrhythmia & Electrophysiology Review, 2014. **3**(1): p. 25-29.

57. Suradi, H.S. and Hijazi, Z.M., *Left atrial appendage closure: outcomes and challenges.* Netherlands Heart Journal, 2017. **25**(2): p. 143-151.

58. Rajwani, A., Shirazi, M.G., Disney, P.J.S., Wong, D.T.L., Teo, K.S.L., et al., *Left Atrial Appendage Eccentricity and Irregularity Are Associated With Residual Leaks After Percutaneous Closure.* JACC: Clinical Electrophysiology, 2015. **1**(6): p. 478-485.

59. Mousa, A.Y., Campbell, J.E., AbuRahma, A.F., and Bates, M.C., *Current update of cerebral embolic protection devices.* Journal of Vascular Surgery, 2012. **56**(5): p. 1429-1437.

60. Masuda, J., Yutani, C., Ogata, J., Kuriyama, Y., and Yamaguchi, T., *Atheromatous embolism in the brain A clinicopathologic analysis of 15 autopsy cases.* Neurology, 1994. **44**(7): p. 1231-1231.

61. Moody, D.M., Brown, W.R., Challa, V.R., Stump, D.A., Reboussin, D.M., et al., *Brain microemboli associated with cardiopulmonary bypass: A histologic and magnetic resonance imaging study.* The Annals of Thoracic Surgery, 1995. **59**(5): p. 1304-1307.

62. DelStar Technologies. *Product Datasheets*. 2017; Available from: http://extrudedfilmsandnets.co.uk/products/datasheets.

63. Baldez, E.E., Robaina, N.F., and Cassella, R.J., *Employment of polyurethane foam for the adsorption of Methylene Blue in aqueous medium.* Journal of Hazardous Materials, 2008. **159**(2): p. 580-586.

APPENDIX A

MECHANICAL PROPERTIES OF SMP FOAM AND THERMOPLASTIC POLYURETHANE FILM

Methodology

The mechanical properties of thermoplastic polyurethane (TPU) film and non-cleaned and non-reticulated H40 foams were investigated. The pore sizes of the foams ranged from small, medium, and large; which corresponded to 1000, 1500, and 1800 μm pore sizes, respectively. The mechanical properties of the TPU films were taken from the manufacturer's website, whereas the mechanical properties of foam were characterized following the ASTM D638 standard for non-rigid samples [62].

To characterize the foams they were first sliced to a thickness ≤ 4mm. A calibrated and certified ASTM D638 Type IV cutter (Pioneer-Dietecs Corporation, Weymouth MA) was used to punch dog bone samples from the foam slices. The ends of the dog bone samples were then epoxied to wooden stubs so they can be attached to the tensile tester's grips. The dog bone samples were then allowed to dry overnight in a vacuum oven. Dried dog bone samples were then loaded onto an Insight 30 material tester (Materials Testing Solutions, MTS Systems Corporation, Eden Prairie, MN), and strained until failure. Each composition was tested at least four times for reproducibility.

Results

Table A-1 and **Figure A-1** summarize the key mechanical properties for TPU film and H40 foam, respectively. The TPU film and H40 foam had similar tensile strengths. Foam pore size significantly affected the strain at break and modulus of foam. Foams with a smaller pore size possessed a lower modulus and were more flexible in a dry state when compared to their larger pore counterparts. Therefore, a small pore foam may enable easier delivery through tortuous anatomy and not fracture as readily. Fracture may occur under extreme strain of the foam, which may occur as the foam is retracted into the catheter. However, no conclusions can be determined at this time since these results reflect the mechanical properties of dry, non-processed foam, and not the mechanical properties of the wet, processed foam used in the clinical setting.

Table A-1: Key mechanical properties of the TPU film compositions used to fabricate SEDs. Taken from [62].

Mechanical Property	AU25 TPU Film	EU28 TPU Film	EU29 TPU Film
Thickness (μm)	23	28	27
Tensile Strength (MPa)	0.079	0.10	0.079
Elongation at Break %	400	650	500

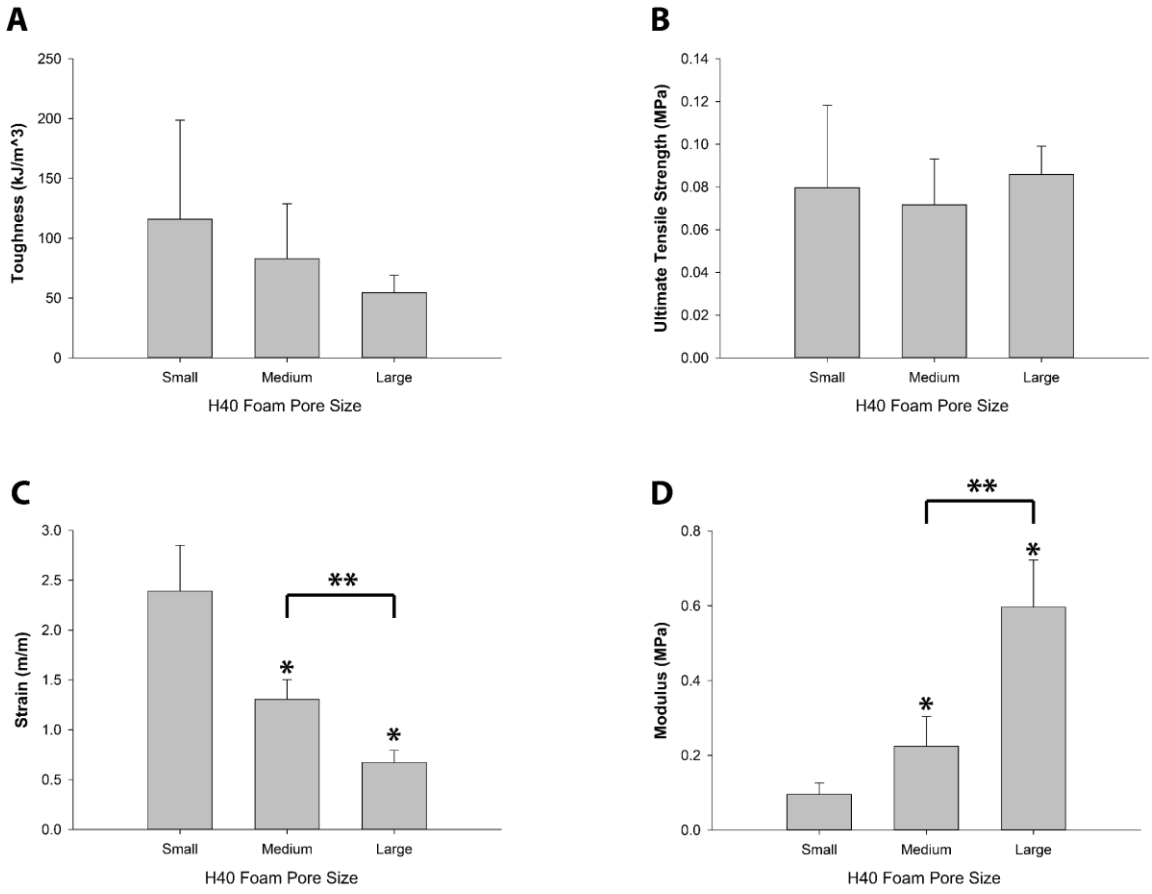

Figure A-1: (A) Toughness, (B) ultimate tensile strength, (C) strain at break, and (D) modulus of H40 foam for varying pore sizes. Small, medium, and large corresponds to a pore size of 1000, 1500, and 1800 µm, respectively. Mean ± standard deviation displayed; N ≥ 4; *p<0.05 relative to small pore foam; **p<0.05 between the bracketed groups.

APPENDIX B

SUMMARY OF ACTUATION SOFTWARE

Purpose

The purpose of developing software was to expedite the process of determining the actuation profiles of SMP foam. Actuation profiles of SMP foams simply refers to the change in shape of SMP foam as a function of time. Prior to the development of this software determining the actuation profiles of SMP foams was a manual-intensive process that could take upwards of 30 minutes and result in variability depending on the user.

Description of software

The software was developed with MATLAB (MATLAB R2015b, The MathWorks Inc., Natick, MA, 2000). A graphical user interface (GUI) was made using MATLAB's built-in features, and allows the user to interactively and intuitively process their images (**Figure B-1**). Briefly, execution of the program brings up a main interactive screen (**Figure B-1A**). The user then uploads all the images to be analyzed. The user then sets a scale that relates pixels to units of length by first entering the known distance then measuring the reference in a pop-up figure (**Figure B-1B**). The user then marks a region of interest around the target of interest (e.g. SMP foam changing shape) (**Figure B-1C**). The region of interest essentially disregards everything outside the region and improves accuracy. The user then selects "Gray Thresh", which isolates the target of interest from

background based on gray-scale intensity values (**Figure B-1D**). The user may fill pores or holes that are present following thresholding (**Figure B-1E**).

The technical details of the program can be summarized as follows: the isolated target of interest (e.g. SMP foam) is converted to a binary image and the 2-D projected surface area is calculated; the surface area is then divided by the length of the target of interest to determine the diameter; the diameter is plotted against time and displayed to the user. The program then exports processed image files and an excel spreadsheet to a user-specified folder. Throughout the process the degree of automation can be managed by the user.

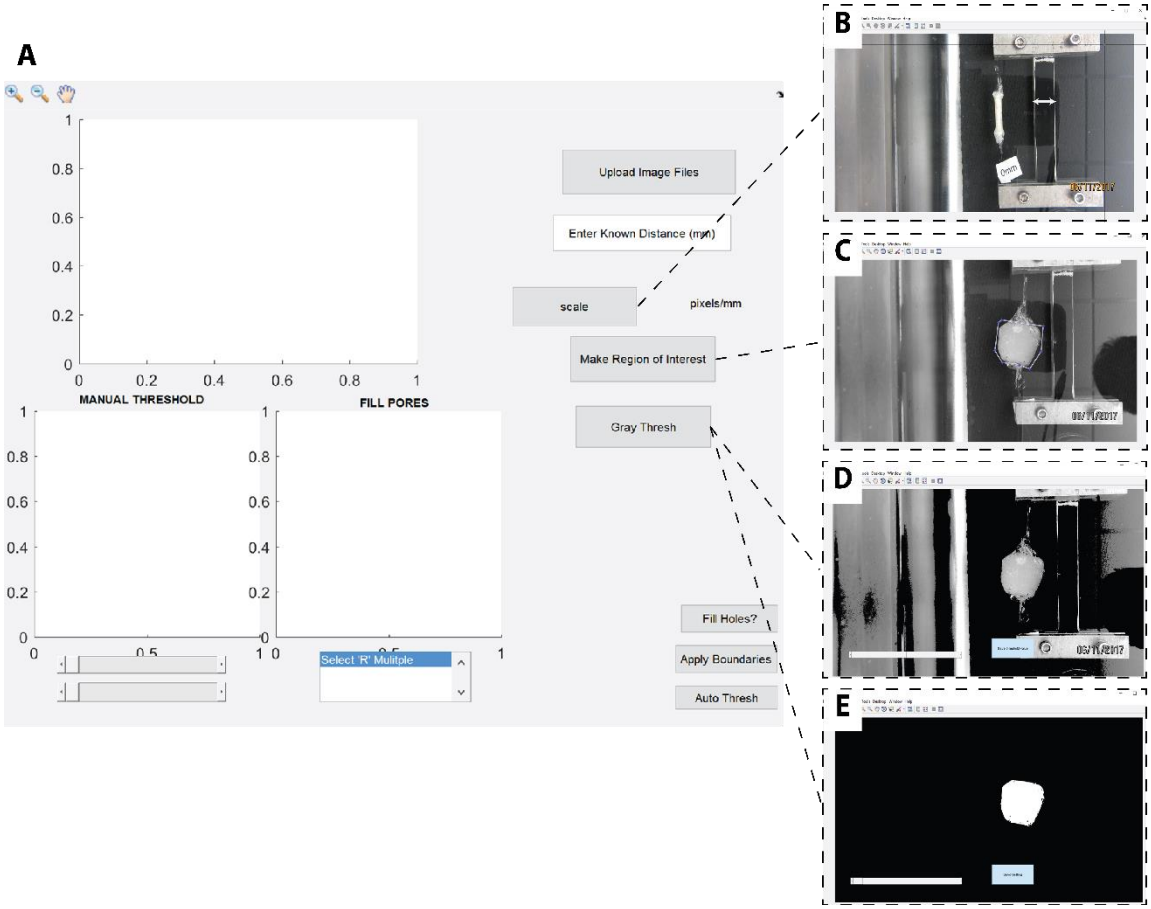

Figure B-1: Interactive GUI to analyze actuation image data: (A) Main user interface (B) figure pop-up to allow user to set scale and measure length of foam (C) figure pop-up to allow user to set region of interest (D) figure pop-up to allow user to isolate foam from background based on gray-scale values (E) figure pop-up to allow user to fill in holes.

APPENDIX C

VERIFICATION OF ACTUATION SOFTWARE

Scope

The purpose of verifying software, in general, is to demonstrate the software is consistent, complete, and correct: verification answers the question “is the software built right?”. Whereas software validation demonstrates that the software is built according to the user requirements and answers the question “did we build the right system?”. Within this thesis software was developed via MATLAB to allow users to extract measurements from images; in particular, the software extracted the average diameters of foam as a function of time. The software was developed to dramatically reduce time when analyzing these image sets. To verify the software, manual measurements were compared to software generated measurements.

Method

Software verification was performed by comparing measurements taken manually and via the software. To do this, images of SMP foam changing shape in a water bath set at 37°C were taken with a digital camera (PowerShot SX230 HS, Canon Inc., Tokyo, Japan) every 30 seconds.

Manual measurements were taken with ImageJ (NIH, Bethesda, MD) open-source software. Each image was analyzed with ImageJ by first setting a scale that relates pixels to a unit of length, then measuring the width of the foam across its length at 15-20 evenly

spaced locations. The width measurements were then averaged to determine the average diameter of the SMP foam at that specific time point. These measurements were then repeated until the entire image set was analyzed. Semi-automated measurements were taken with the MATLAB program described in Appendix B. Global settings were applied when analyzing images in the MATLAB program, as opposed to individual settings (e.g. individual thresholding vs. universal thresholding).

Results and discussion

Manual and semi-automated measurements taken with ImageJ and the MATLAB program were plotted against each other to determine if there is a relationship between the two methods. **Figure C-1** shows a positive linear correlation between both methods of measurements ($R^2 > 0.99$). Two samples with different actuation profiles were investigated to demonstrate the robustness of the program. Furthermore, the samples used in this verification study were SED's, which added complexity to the measurements due to the varying degrees of contrast in the images. Verification was also performed on individual SMP foams (not shown), and also demonstrated a positive linear correlation between both methods. The results presented herein demonstrate that the semi-automated MATLAB program can be used in substitution of manual measurements to expedite actuation analysis.

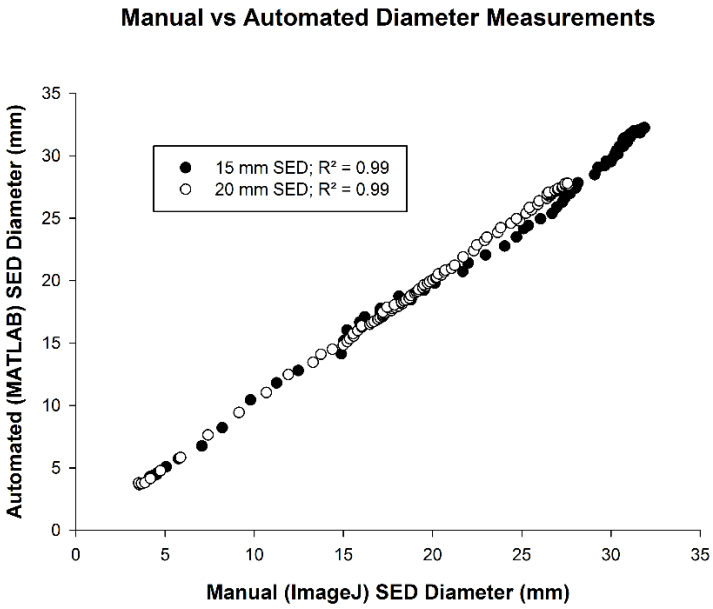

Figure C-1: Comparison of SED diameter as measured by manually (ImageJ) or automatically (MATLAB program).

APPENDIX D

FOAM EXPANSION ANALYSIS

Scope

An index was calculated to identify if pore size or bore size affected foam expansion. The index was taken as the time at which the foam was 50% expanded. The index was then compared as a function of pore and bore size.

Method

An exponential or polynomial curve was fitted to the experimental ‘diameter vs time’ data. Using the equation corresponding to the fitted curves, the time at which the foam expanded to 50% of its final diameter was calculated.

Results

A two-way ANOVA was performed to determine if pore or bore size significantly affected the index, and as a result, the expansion rate of foams. Results show no statistical significance due to either bore or pore size. **Figure D-1** shows the averaged index as a function of bore and pore size.

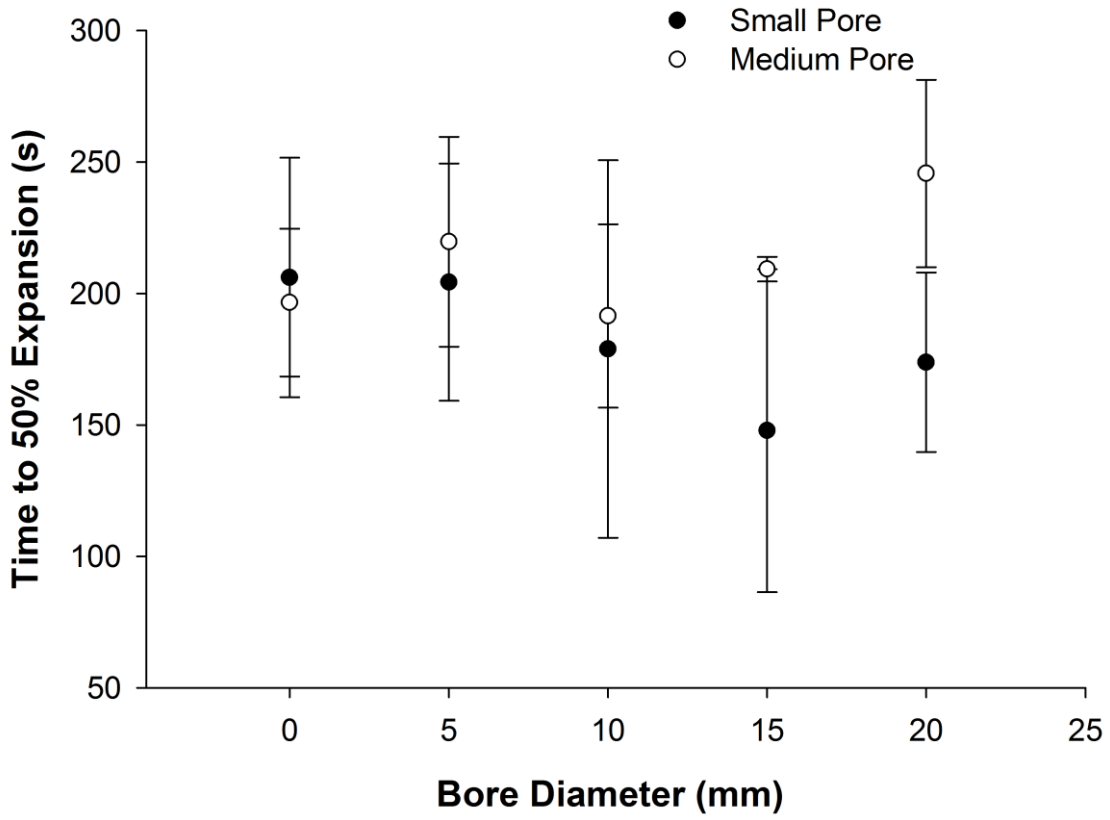

Figure D-1: The time for foam to reach 50% of its expanded diameter, referred to as "index", as a function of pore and bore size (N ≥ 2).

APPENDIX E

DYEING POLYURETHANE FOAM

Scope

To improve manual and automated counting of particles using the microscope method the contrast between the particles and background should be sufficient. This can be achieved by purchasing colored filters or, alternatively, dyeing the particles. In this research, polyurethane foams were dyed to improve particle counting.

Method

A protocol based on Baldez et al. was adapted to dye our polyurethane foams [63]. Briefly, a solution of sodium dodecyl sulfate (SDS) and Nile Blue (NB) was made at a molar concentration of 4:1, respectively. Polyurethane foams were then placed into the solution and gently stirred for at least 100 minutes to allow uptake of dye. The foams were then removed, blotted, and then placed into an oven at 80°C overnight to dry. Following drying the foams can be rinsed to remove residual dye, or used as is.